# The SARS-CoV-2 Lambda variant exhibits enhanced infectivity and immune resistance

AUTHOR(S):

Kimura, Izumi; Kosugi, Yusuke; Wu, Jiaqi; Zahradnik, Jiri; Yamasoba, Daichi; Butlertanaka, Erika P.; Tanaka, Yuri L.; ... Saito, Akatsuki; Nakagawa, So; Sato, Kei

CITATION:

Kimura, Izumi ...[et al]. The SARS-CoV-2 Lambda variant exhibits enhanced infectivity and immune resistance. Cell Reports 2022, 38(2): 110218.

ISSUE DATE:

2022-01

URL:

http://hdl.handle.net/2433/267436

Report

Cell Reports

# The SARS-CoV-2 Lambda variant exhibits enhanced infectivity and immune resistance

## Graphical abstract

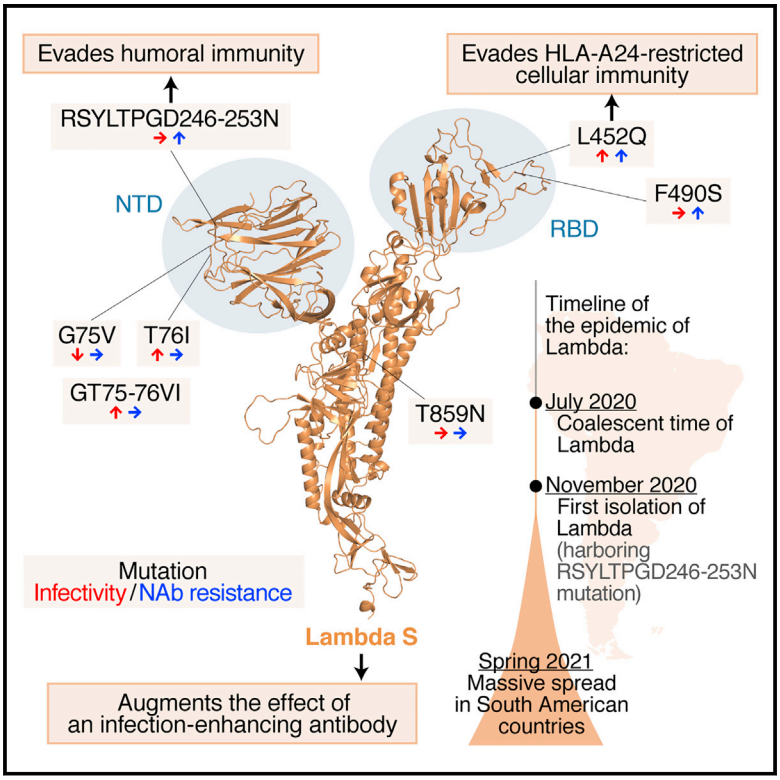


## Highlights

- Insertion of RSYLTPGD246-253N mutation in Lambda S associates with Lambda outbreak
- Lambda S is highly infectious, and T76I and L452Q are responsible for this property
- Lambda S is more susceptible to an infection-enhancing antibody than parental S
- RSYLTPGD246-253N, L452Q, and F490S confer resistance to antiviral immunity

## Authors

Izumi Kimura, Yusuke Kosugi, Jiaqi Wu, ..., Akatsuki Saito, So Nakagawa, Kei Sato

## Correspondence

so@tokai.ac.jp (S.N.), KeiSato@g.ecc.u-tokyo.ac.jp (K.S.)

## In brief

Kimura et al. reveal the characteristics of the SARS-CoV-2 Lambda variant of interest. Lambda spike is more infectious than that of other variants due to the T76I and L452Q mutations. The RSYLTPGD246-253N mutation is responsible for evasion from neutralizing antibodies and further augments antibody-mediated enhancement of infection.

Kimura et al., 2022, Cell Reports *38*, 110218
January 11, 2022 
https://doi.org/10.1016/j.celrep.2021.110218

CellPress

Cell Reports

CellPress OPEN ACCESS

Report

# The SARS-CoV-2 Lambda variant exhibits enhanced infectivity and immune resistance

Izumi Kimura,[1,20] Yusuke Kosugi,[1,2,3,20] Jiaqi Wu,[4,5,20] Jiri Zahradnik,[6] Daichi Yamasoba,[1,7] Erika P. Butlertanaka,[8] Yuri L. Tanaka,[8] Keiya Uriu,[1,9] Yafei Liu,[10,11] Nanami Morizako,[8] Kotaro Shirakawa,[12] Yasuhiro Kazuma,[12] Ryosuke Nomura,[12] Yoshihito Horisawa,[12] Kenzo Tokunaga,[13] Takamasa Ueno,[14] Akifumi Takaori-Kondo,[12] Gideon Schreiber,[6] Hisashi Arase,[9,10,15] The Genotype to Phenotype Japan (G2P-Japan) Consortium, Chihiro Motozono,[14] Akatsuki Saito,[8,16,17] So Nakagawa,[4,5,18,*] and Kei Sato[1,5,9,19,21,*]

[1]Division of Systems Virology, Department of Infectious Disease Control, International Research Center for Infectious Diseases, The Institute of Medical Science, The University of Tokyo, Tokyo 1088639, Japan
[2]Laboratory of Systems Virology, Institute for Frontier Life and Medical Sciences, Kyoto University, Kyoto 6068507, Japan
[3]Graduate School of Pharmaceutical Sciences, Kyoto University, Kyoto 6068501, Japan
[4]Department of Molecular Life Science, Tokai University School of Medicine, Isehara, Kanagawa 2591193, Japan
[5]CREST, Japan Science and Technology Agency, Saitama 3220012, Japan
[6]Department of Biomolecular Sciences, Weizmann Institute of Science, Rehovot 76100, Israel
[7]Faculty of Medicine, Kobe University, Hyogo 6500017, Japan
[8]Department of Veterinary Science, Faculty of Agriculture, University of Miyazaki, Miyazaki 8892192, Japan
[9]Graduate School of Medicine, The University of Tokyo, 1130033 Tokyo, Japan
[10]Department of Immunochemistry, Research Institute for Microbial Diseases, Osaka University, Osaka 5650871, Japan
[11]Laboratory of Immunochemistry, World Premier International Immunology Frontier Research Centre, Osaka University, Osaka 5650871, Japan
[12]Department of Hematology and Oncology, Graduate School of Medicine, Kyoto University, Kyoto 6068507, Japan
[13]Department of Pathology, National Institute of Infectious Diseases, Tokyo 1628640, Japan
[14]Division of Infection and immunity, Joint Research Center for Human Retrovirus infection, Kumamoto University, Kumamoto 8600811, Japan
[15]Center for Infectious Disease Education and Research, Osaka University, Osaka 5650871, Japan
[16]Center for Animal Disease Control, University of Miyazaki, Miyazaki 8892192, Japan
[17]Graduate School of Medicine and Veterinary Medicine, University of Miyazaki, Miyazaki 8892192, Japan
[18]Bioinformation and DDBJ Center, National Institute of Genetics, Mishima, Shizuoka 4118540, Japan
[19]Twitter: @SystemsVirology
[20]These authors contributed equally
[21]Lead contact
*Correspondence: so@tokai.ac.jp (S.N.), KeiSato@g.ecc.u-tokyo.ac.jp (K.S.)
https://doi.org/10.1016/j.celrep.2021.110218

## SUMMARY

SARS-CoV-2 Lambda, a variant of interest, has spread in some South American countries; however, its virological features and evolutionary traits remain unclear. In this study, we use pseudoviruses and reveal that the spike protein of the Lambda variant is more infectious than that of other variants due to the T76I and L452Q mutations. The RSYLTPGD246-253N mutation, a unique 7-amino acid deletion in the N-terminal domain of the Lambda spike protein, is responsible for evasion from neutralizing antibodies and further augments antibody-mediated enhancement of infection. Although this mutation generates a nascent N-linked glycosylation site, the additional N-linked glycan is dispensable for the virological property conferred by this mutation. Since the Lambda variant has dominantly spread according to the increasing frequency of the isolates harboring the RSYLTPGD246-253N mutation, our data suggest that the RSYLTPGD246-253N mutation is closely associated with the substantial spread of the Lambda variant in South America.

## INTRODUCTION

During the current pandemic, severe acute respiratory syndrome coronavirus 2 (SARS-CoV-2), the causative agent of coronavirus disease 2019 (COVID-19), has diversified. As of December 2021, there are 5 variants of concern (VOCs)—Alpha (B.1.1.7 lineage; the lineage classification is based on Phylogenetic Assignment of Named Global Outbreak [PANGO] [https://cov-lineages.org/resources/pangolin.html]), Beta (B.1.351 lineage), Gamma (P.1 lineage), Delta (B.1.617.2 and AY lineages), and Omicron (B.1.1.529 lineage)—and 2 variants of interest (VOIs)—Lambda (C.37 lineage) and Mu (B.1.621 lineage) (WHO, 2021a). These variants are considered potential threats to human society.

VOCs and VOIs harbor multiple mutations in their spike (S) protein and are relatively resistant to neutralizing antibodies (NAbs) that are elicited in convalescent and vaccinated individuals (Chen et al., 2021; Collier et al., 2021; Garcia-Beltran et al., 2021; Hoffmann et al., 2021; Liu et al., 2021a, 2021b; Planas et al., 2021; Wall et al., 2021; Wang et al., 2021a, 2021b). Because the receptor-binding domain (RBD) of the SARS-CoV-2 S protein is the major site that NAbs recognize, mutations in this domain can lead to immune evasion (Piccoli et al., 2020). In addition, mutations in the N-terminal domain (NTD) of the SARS-CoV-2 S protein are associated with neutralization escape (McCallum et al., 2021). Moreover, antibodies that enhance viral infectivity (enhancing antibodies [EAbs]) were detected in severe COVID-19 patients, and these EAbs target the NTD (Li et al., 2021; Liu et al., 2021c). Because natural mutations in the S NTD crucially influence the sensitivity to antibodies (Gobeil et al., 2021), the accumulation of mutations in this domain is closely associated with the infectious spread of VOCs and VOIs.

The Lambda variant (also known as the C.37 lineage) was classified as a VOI on June 14, 2021 (WHO, 2021a) and has spread in South American countries such as Peru, Chile, Argentina, and Ecuador (WHO, 2021a). Based on the data from the Global Initiative on Sharing All Influenza Data (GISAID) database (https://www.gisaid.org; as of June 29, 2021), the Lambda variant has been isolated in 26 countries. Notably, the vaccination rate in Chile is relatively high; the percentage of people who received at least one dose of COVID-19 vaccine was ~60% on June 1, 2021 (https://ourworldindata.org/covid-vaccinations). A recent article also suggested that vaccines have effectively prevented COVID-19 in Chile (Jara et al., 2021). Nevertheless, a large COVID-19 surge occurred in Chile in spring 2021 (WHO, 2021b), suggesting that the Lambda variant can effectively escape from the antiviral immunity elicited by vaccination. In this study, we reveal the evolutionary traits of the Lambda variant by molecular phylogenetic analysis. We further demonstrate that the RSYLTPGD246-253N mutation, a unique mutation in the NTD of the Lambda S protein, is responsible for the virological phenotype of the Lambda variant that is associated with the major infectious spread mainly in South American countries.

## RESULTS

### Epidemic dynamics of the Lambda variant in South American countries

As of June 29, 2021, 1,908 genome sequences of the Lambda variant belonging to the PANGO C.37 lineage have been isolated from 26 countries and deposited in GISAID. Although the Lambda variant was first reported in Peru in December 2020 (WHO, 2021a), our in-depth analysis revealed that this variant was first detected in Argentina on November 8, 2020 (GISAID: EPI_ISL_2158693) (Figure 1A; see STAR Methods for details). The prevalence of the Lambda variant is increasing in South American countries, including Peru, Chile, and Argentina (Figure 1A and Table S1), suggesting that this variant is spreading predominantly in these countries (Table S2). We then generated a maximum likelihood-based phylogenetic tree of the Lambda variant (Figure S1A). Although there were some isolates that were misclassified as Lambda, which could be the "sister group of Lambda variants," our phylogenetic tree indicated the monophyly of the "genuine Lambda variants" isolates (Figure S1A).

### Association of the Lambda variant spread with the increasing frequency of isolates harboring the RSYLTPGD246-253N mutation

In the 1,908 sequences of the Lambda variant (C.37 lineage), the majority of the S protein sequence of the genuine Lambda variants contains 6 substitution mutations (G75V, T76I, L452Q, F490S, D614G, and T859N) and a 7-amino acid deletion in the NTD (RSYLTPGD246-253N) (Figure S1A). The Lambda variant first isolated in Argentina contains the 6 amino acid mutations as well as the deletion in the S protein. However, the sister group of Lambda variants does not contain any of the 7 mutations, excluding D614G in their S proteins (Figure S1A).

We then analyzed the mutations in the S protein using the 1,908 sequences of the Lambda variant (C.37 lineage) and showed that the 6 amino acid mutations are highly (>90%) conserved (Figure 1B). Although a large deletion in the NTD, the RSYLTPGD246-253N mutation, is also highly conserved, and only 287 of the 1,908 sequences (15.0%) of the Lambda variant (C.37 lineage) genomes do not harbor this mutation (Figures 1B and S1A). To determine whether the epidemic dynamic of the Lambda variant is associated with the emergence of the RSYLTPGD246-253N mutation, we examined all of the amino acid changes in the S protein of the SARS-CoV-2 genomes deposited in the GISAID database (2,084,604 sequences; as of June 29, 2021). Our analysis showed that the RSYLTPGD246-253N mutation was first found in Argentina on November 8, 2020, which is the first isolate of the Lambda variant (Figure 1A), suggesting that this deletion event uniquely occurred in the ancestral lineage of the genuine Lambda variants. We then analyzed the molecular evolutionary dynamics of the Lambda variants by performing Bayesian tip-dating analysis. We showed that the estimated time to the most recent common ancestor of the genuine Lambda variants was approximately July 12, 2020 (95% highest posterior density [HPD], January 5, 2020–October 22, 2020) (Figures 1C and S1B). To infer the population dynamics of the lineage, we performed a Bayesian skyline plot analysis. This analysis showed that the effective population size of the Lambda variant increased at the beginning of 2021 (Figure 1D). Intriguingly, when we plotted the proportion of the Lambda variant with the RSYLTPGD246-253N mutation, we found that it increased after the emergence of the Lambda variant and closely associated with the increase in effective population size (Figure 1D). These results suggest that the acquisition of the RSYLTPGD246-253N mutation is associated with the outbreak of the Lambda variant in South America.

### Enhanced infectivity and resistance to NAbs of the Lambda variant

To address the virological phenotype of the Lambda variant (hereafter, only genuine Lambda variant is referred to as "Lambda variant"), we prepared viruses pseudotyped with the S proteins of the Lambda variant as well as 4 VOCs, Alpha (B.1.1.7), Beta (B.1.351), Gamma (P.1) and Delta (B.1.617.2) (Figure S1C). We also prepared pseudoviruses with the S protein of the Epsilon (B.1.427/429) variant (Figure S1C), which was used

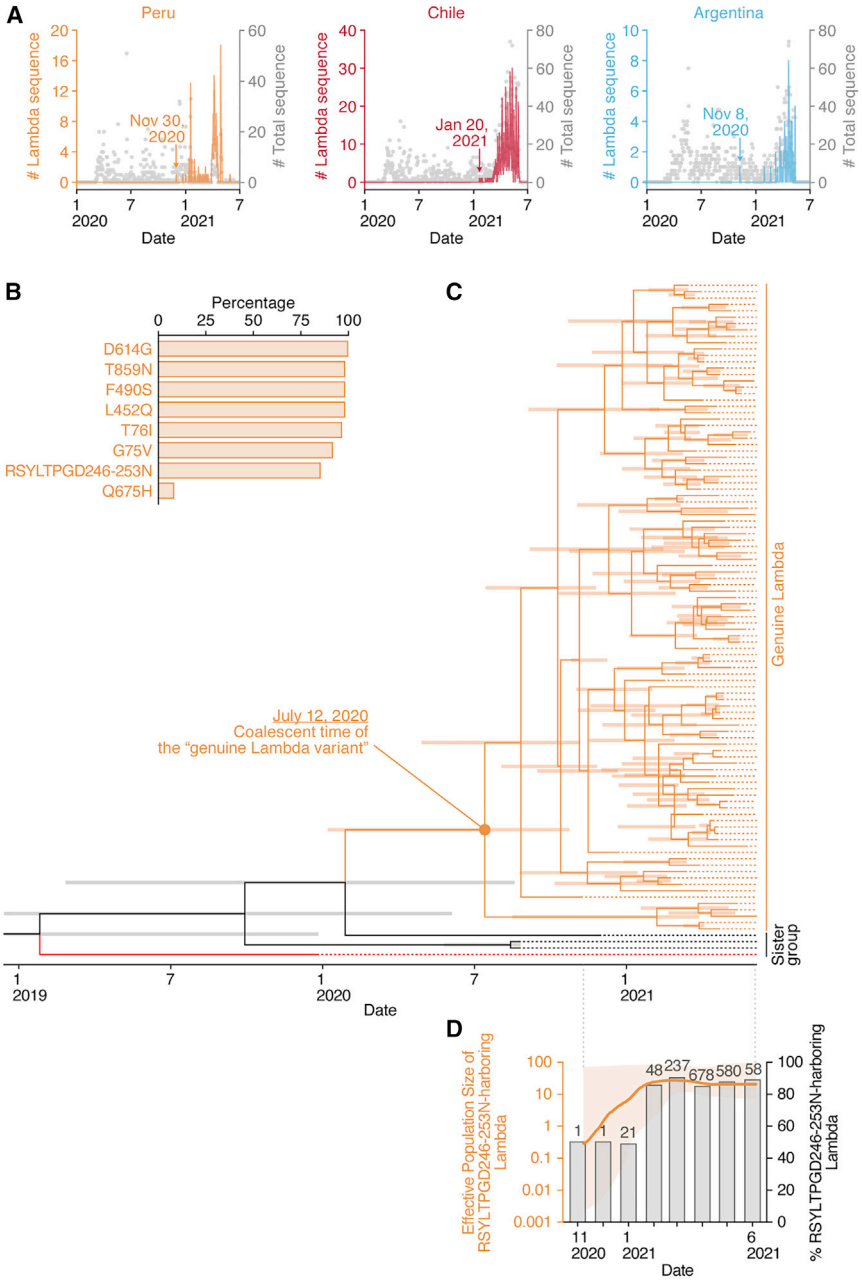


**Figure 1. Epidemic and evolutionary dynamics of the Lambda variant**

(A) Epidemic dynamics of the Lambda variant in three South American countries. The numbers of the Lambda variant (C.37 lineage) sequences deposited per day from Peru (brown), Chile (dark red), and Argentina (pale blue) are indicated by lines. Gray dots indicate the numbers of SARS-CoV-2 genome sequences deposited in the GISAID database per day from the indicated countries. The raw data are summarized in Tables S1 and S2.

(B) Proportion of amino acid replacements in the Lambda variant (C.37 lineage). The top 8 replacements conserved in the S protein of the Lambda variant (C.37 lineage) are summarized. The raw data are summarized in Table S3.

(C) An evolutionary timetree of the Lambda variant (C.37 lineage). The coalescent time of the genuine Lambda variants is indicated in the figure. The 3 sequences (GISAID: EPI_ISL_1,532,199 [B.1.1.1 lineage], EPI_ISL_1,093,172 [B.1.1.1 lineage], and EPI_ISL_1,534,656 [C.37 lineage]) and the sister group of Lambda variants are indicated in black. Wuhan-Hu-1 (GISAID: EPI_ISL_1,532,199), the oldest SARS-CoV-2 (isolated on December 26, 2019), is indicated in red. Bars on the internal nodes correspond to the 95% HPD. The tree noted with the GISAID ID and sampling date at each terminal node is shown in Figure S1B.

(D) Transition of the effective population size of the Lambda variant and the proportion of the Lambda variant harboring the RSYLTPGD246-253N mutation. The effective population size of the Lambda variant harboring the RSYLTPGD246-253N mutation (left y axis) was analyzed by a Bayesian skyline plot. The initial date was when the first Lambda variant was sampled (November 8, 2020). The 95% HPD is shaded in brown. In the same panel, the proportion of the Lambda variants harboring the RSYLTPGD246-253N mutation for each month (right y axis) is also plotted. The number at each time point indicates the number of Lambda variants harboring the RSYLTPGD246-253N mutation. The number in parentheses indicates the number of Lambda variants deposited in the GISAID database. See also Figure S1 and Tables S1, S2, and S3.

as a VOC/VOI and was reclassified on July 6, 2021 (WHO, 2021a). As the control of this experiment, the pseudoviruses with the S protein of the D614G-bearing isolate (B.1 lineage), which spread in the early pandemic (i.e., during early 2020 and before the emergence of VOCs/VOIs) (Ozono et al., 2021), were prepared, and this is referred to as "parental virus" in this study. As shown in Figure 2A, the infectivities of the Alpha and Beta variants were significantly lower than that of the parental virus ($p = 0.0012$, Alpha versus parental; $p = 0.0012$, Beta versus parental by Student's t test), and the infectivities of the Gamma variant and the parental virus were comparable. Since the epidemic of SARS-CoV-2 in the early pandemic, which includes the B.1 lineage (parental virus in this study), was outcompeted by VOCs including the Alpha and Beta variants during late 2020 (WHO, 2021a), it was unexpected that the infectivities of Alpha and Beta variants were lower than that of the parental virus (Figure 2A). However, the lower infectivity of the Alpha variant compared to the D614G-bearing early pandemic virus, analyzed by pseudovirus assay (Figure 2A), is consistent with a previous report (Acevedo et al., 2021). In contrast, the infectivities of the Delta, Epsilon, and Lambda variants were significantly higher than that of the parental virus (Figure 2A: $p = 0.017$, Delta versus

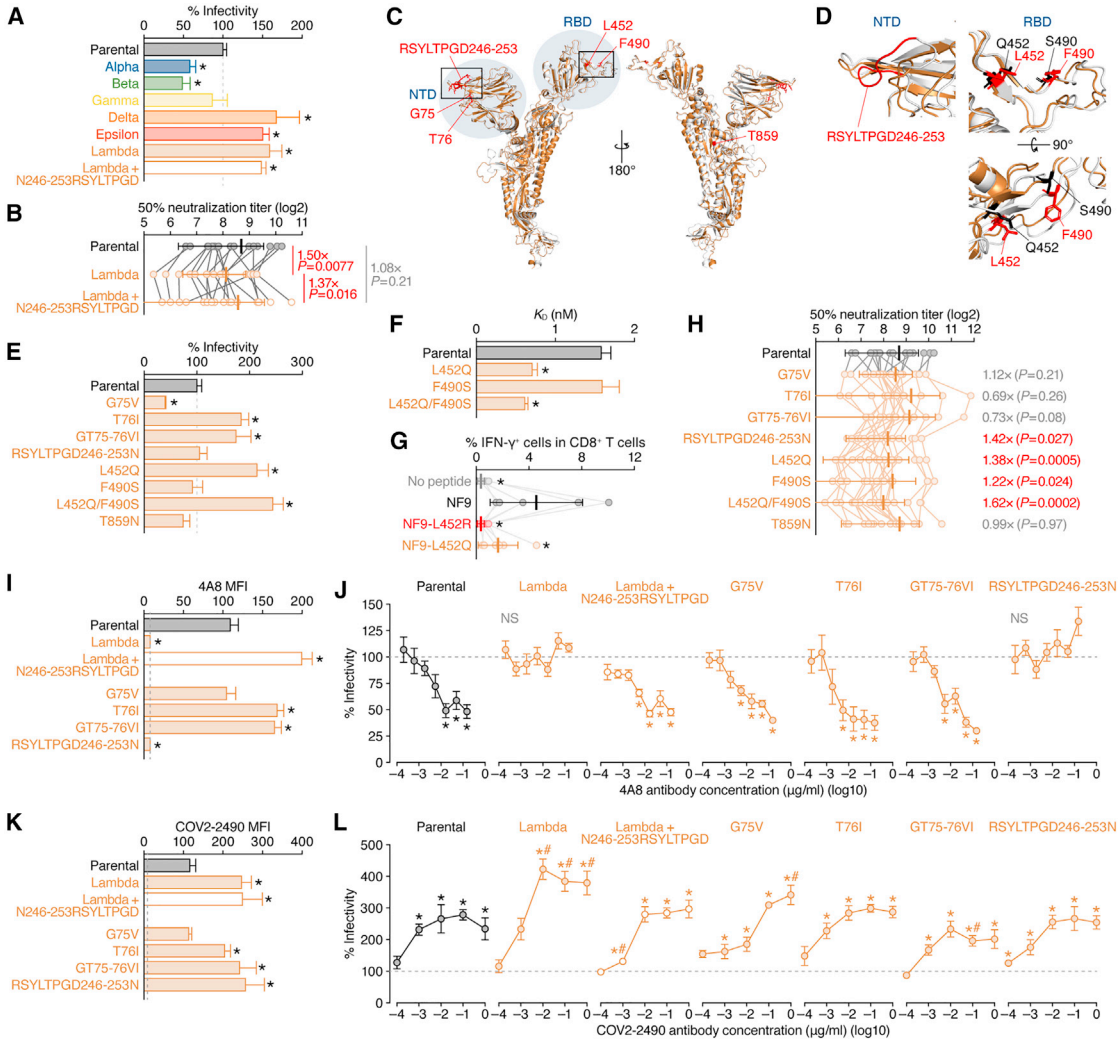


**Figure 2. Virological and immunological features of the Lambda variant**

(A) Pseudovirus assay. HIV-1-based reporter viruses pseudotyped with SARS-CoV-2 S proteins of the parental (B.1), Alpha (B.1.1.7), Beta (B.1.351), Gamma (P.1), Delta (B.1.617.2), Epsilon (B.1.427), and Lambda (C.37) variants and the Lambda + N246-253RSYLTPGD derivative were prepared as described in STAR Methods. The mutations in each variant are listed in Figure S1C. The pseudoviruses were inoculated in HOS-ACE2/TMPRSS2 cells at 1,000 ng HIV-1 p24 antigen, and the percentages of infectivity compared to that of the virus pseudotyped with parental S are shown.

(B) Neutralization assay. A neutralization assay was performed using the pseudoviruses with the S proteins of the parental, Lambda, and Lambda + N246-253RSYLTPGD and 18 BNT162b2-vaccinated sera as described in STAR Methods. The raw data are shown in Figure S2B. The number in the panel indicates the fold change in neutralization resistance of Lambda S to the parental S or the Lambda + N246-253RSYLTPGD derivative.

(C and D) Structural insights of the mutations in Lambda S. (C) Overlaid overviews of the crystal structure of SARS-CoV-2 S (PDB: 6ZGE, white) (Wrobel et al., 2020) and a homology model of Lambda S (brown) are shown. The mutated residues in the Lambda S and the regions in the NTD and RBD are indicated in red and blue. The squared regions are enlarged in (D). Mutated residues in the NTD (left) and RBD (right) of Lambda S. The residues in parental S and the Lambda S are indicated in red and black.

(E) Pseudovirus assay. HIV-1-based reporter viruses pseudotyped with SARS-CoV-2 S proteins bearing respective mutations of the Lambda variant in parental S (G75V, T76I, GT75-76VI, RSYLTPGD246-253N, L452Q, F490S, L452Q/F490S, or T859N) as well as the parental S were prepared. The pseudoviruses were inoculated into HOS-ACE2/TMPRSS2 cells at 1,000 ng HIV-1 p24 antigen, and the percentages of infectivity compared to that of the virus pseudotyped with parental S are shown.

(F) Binding affinity of the SARS-CoV-2 S RBD (residues 336-528) to ACE2 by yeast surface display. The $K_D$ values of the binding of the SARS-CoV-2 S RBD expressed on yeast to soluble ACE2 are shown.

(G) CTL assay. HLA-A24$^+$ CTL lines established from 6 BNT162b2-vaccinated donors were stimulated with 1 nM NF9 peptide or its derivatives, NF9-L452Q (NYNYQYRLF) or NF9-L452R (NYNYRYRLF). The percentage of IFN-$\gamma^+$ cells in CD8$^+$ T cells (bottom, n = 6) is shown. Representative fluorescence-activated cell sorting (FACS) plots showing intracellular expression of IFN-$\gamma$ in the CD8$^+$ T cell subset of a vaccinated donor (top, donor GV36-2) are shown in Figure S2H.

(H) Neutralization assay. A neutralization assay was performed using the pseudoviruses used in Figure 2B and 18 BNT162b2-vaccinated sera, as described in STAR Methods. The raw data are shown in Figure S2B. The number in the panel indicates the fold change in neutralization resistance to the parental S.

*(legend continued on next page)*

parental; p = 0.0031, Epsilon versus parental; p = 0.0004, Lambda versus parental by Student's t test). This pattern was independent of the input dose of pseudoviruses used (Figure S2B).

To assess the effect of a characteristic mutation of the Lambda variant, the RSYLTPGD246-253N mutation (Figure 1), on viral infectivity, we prepared a pseudovirus with the Lambda S derivative with the recovery of this deletion (Lambda + N246-253RSYLTPGD) (Figure S2A). The infectivity of this mutant was comparable to that of the Lambda S (Figures 2A and S2B). To further verify the effect of the N246-253RSYLTPGD mutation on the infectivity of the Lambda variant, we prepared the fluorescent protein-expressing lentivirus vectors pseudotyped with Lambda S (expressing Crimson) and Lambda + N246-253RSYLTPGD S (expressing ZsGreen1). The competition assay using these fluorescent protein-expressing pseudoviruses showed that both viruses exhibit similar infectivities (Figure S2C), suggesting that the 7-amino acid deletion in the NTD does not affect viral infection.

Because NAb resistance is a notable phenotype of most VOCs (reviewed in Harvey et al., 2021), we next analyzed the sensitivity of Lambda S to NAbs induced by BNT162b2 vaccination (Table S4). As shown in Figure 2B, Lambda S was, on average, 1.5-fold (2.63-fold at a maximum) more resistant to BNT162b2-induced antisera than the parental S (p = 0.0077 by the Wilcoxon matched-pairs signed rank test). However, the neutralization level of Lambda + N246-253RSYLTPGD was similar to that of the parental S pseudovirus (P = 0.21 by the Wilcoxon matched-pairs signed rank test), and this recovered variant was 1.37-fold more sensitive to vaccine-induced neutralization than the Lambda variant (P = 0.016 by the Wilcoxon matched-pairs signed rank test) (Figures 2B and S2D). These results suggest that Lambda S is highly infectious and resistant to vaccine-induced humoral immunity, and the robust resistance of Lambda S to vaccine-induced neutralization is determined by a 7-amino acid deletion in the NTD.

## Effect of consensus mutations in Lambda S on viral infectivity

We next examined 6 substitution mutations (G75V, T76I, L452Q, F490S, D614G, and T859N) and a deletion mutation (RSYLTPGD246-253N) of the Lambda variant in the structure of the SARS-CoV-2 S protein. Structural analysis showed that the 3 mutations, G75V, T76I, and RSYLTPGD246-253N, are in the NTD (Figure 2C), and the RSYLTPGD246-253N mutation is located in a loop structure, which was designated as loop 5 (residues 246–260) in a previous study (Chi et al., 2020) (Figure 2D). The G75V and T76I mutations are located at the flexible loop adjacent to loop 5 (Figure 2C). The L452Q and F490S mutations are situated in the receptor-binding motif in the RBD (Figures 2C and 2D), but neither residue is in direct contact with the angiotensin-converting enzyme 2 (ACE2) receptor (Figure S2E). The T859N mutation is in the heptad repeat 1 of the S2 subunit (Figure 2C).

To investigate the effects of these seven consensus mutations in Lambda S on viral infectivity and NAb sensitivity, we prepared viruses pseudotyped with parental S-based derivatives that have mutations of the Lambda variant. Figure 2E shows that the G75V mutation significantly reduces viral infectivity (p = 0.0004, by Student's t test), while the T76I and GT75-76VI mutations significantly increase viral infectivity (p = 0.0011, T75I versus parental; p = 0.012, GT75-76TI versus parental by Student's t test). In addition, 91.5% (1,746/1,908) of the Lambda variant sequences had these 2 mutations, and the phylogenetic tree of the Lambda variant indicated that the variant harboring either G75V or T76I sporadically emerged during the epidemic of the Lambda variant (Figure S1A). However, there were no viral sequences harboring the G75V mutation without the T76I mutation (Figure S1A). These findings suggest that T76I is a compensatory mutation to recover the decreased infectivity by the G75V mutation.

Similar to the results from the experiment using pseudoviruses with Lambda S and Lambda + N246-253RSYLTPGD (Figure 2A), the insertion of the RSYLTPGD246-253N mutation did not affect viral infectivity (Figure 2E). The infectivity of the T859N mutation was also similar to that of the parental pseudovirus (Figure 2E). When we focused on the effect of the mutations in the RBD, the L452Q and L452Q/F490S mutations significantly increased viral infectivity (p = 0.0011, L452Q versus parental; p = 0.0003, L452Q/F490S versus parental by Student's t test), while the F490S mutation did not (Figure 2E). In addition, the binding affinity of the SARS-CoV-2 RBD to soluble ACE2 was significantly increased by the insertion of the L452Q mutation, but not the F490S mutation (Figure 2F: p = 0.0004, L452Q versus parental; p = 0.92, F490S versus parental; p = 0.0002, L452Q/F490S versus parental by Student's t test). These results suggest that the T76I and L452Q mutations are responsible for the higher infectivity of Lambda S (Figure 2E). The effect of each mutation was similar with different amounts of pseudoviruses used and in the target cells without TMPRSS2 expression (Figure S2F).

(I–L) Effect of monoclonal antibodies. The mean florescence intensity (MFI) of the surface S proteins stained with NTD-targeting NAb clone 4A8 (151 ng/mL–0.21 ng/mL) (Chi et al., 2020) (I) and EAb clone COV2-2490 (1 μg/mL–0.10 μg/mL) (Liu et al., 2021c) (K) antibodies. (J) Antiviral effect of the NTD-targeting NAb clone 4A8 antibody. (L) Enhancing effect of the EAb clone COV2-2490 antibody. The percentages of infectivity compared to that of the virus without antibodies are shown.

Assays were performed in triplicate (except for H) or quadruplicate (H), and the mean is shown with the SD.

In (A), (E), (F), (I), and (K), statistically significant differences (*, p < 0.05) versus parental S were determined by Student's t test. In (A) and (E), vertical dashed lines indicate 100% (the value of parental S).

In (B) and (H), statistically significant differences were determined by the Wilcoxon matched-pairs signed rank test. The p values are indicated in the figure.

In (G), statistically significant differences (*p < 0.05) versus the NF9 peptide were determined by the Wilcoxon matched-pairs signed rank test.

In (I) and (K), vertical dashed lines indicate the MFIs of mock-transfected cells. In (J), statistically significant differences (*p < 0.05) versus the value without the antibody were determined by Student's t test. NS, no statistical significance. In (L), statistically significant differences versus the value without the antibody (*p < 0.05) and the parental S (#p < 0.05) were determined by Student's t test.

See also Figure S2 and Tables S4 and S5.

### Evasion of vaccine-induced cellular immunity induced by the L452Q mutation

Previous studies showed that the 9-mer peptide spanning the 448–456 residues of the SARS-CoV-2 S protein (designated NF9) is an immunodominant epitope presented by human leukocyte antigen (HLA)-A24 in convalescent individuals with SARS-CoV-2 infection (Gao et al., 2021; Hu et al., 2021; Kared et al., 2021). Interestingly, we recently demonstrated that the L452R mutation, a hallmark mutation in the Delta and Epsilon variants, could induce evasion of the antiviral effects triggered by HLA-A24-restricted cytotoxic T lymphocytes (CTLs) (Motozono et al., 2021). To determine whether the L452Q mutation in the Lambda variant can contribute to evasion of HLA-A24-restricted anti-SARS-CoV-2 cellular immunity, as in the case of the L452R mutation (Motozono et al., 2021), we obtained peripheral blood mononuclear cells (PBMCs) from HLA-A*24:02$^{+}$ individuals vaccinated with BNT162b2 and stimulated these cells with the NF9 peptide (Table S5). As shown in Figure S2G, the NF9 peptide activated the PBMCs from HLA-A*24:02$^{+}$ vaccinated individuals, but not those from HLA-A*24:02$^{-}$ vaccinated individuals or HLA-A*24:02$^{+}$ unvaccinated individuals, suggesting that the NF9 peptide is an immunodominant epitope for PBMCs from HLA-A*24:02$^{+}$ BNT162b2-vaccinated individuals. We then assessed whether the L452Q mutation evades the HLA-A24-restricted cellular immunity induced by BNT162b2 vaccination. Consistent with our previous study (Motozono et al., 2021), the NF9 peptide significantly induced interferon-$\gamma$ (IFN-$\gamma$) production (Figures 2G and S2H: $p = 0.031$ by the Wilcoxon matched-pairs signed rank test). In sharp contrast, 2 substitutions of the NF9 peptide, NF9-L452R and NF9-L452Q, faintly activated the NF9-specific CTLs (Figures 2G and S2H). These results suggest that the NF9 peptide is an immunodominant epitope in HLA-A*24:02$^{+}$ vaccinated individuals and that the L452Q mutation potentially results in evasion of HLA-A24-restricted cellular immunity.

### Evasion of vaccine-induced humoral immunity

We next assessed the sensitivity of these pseudoviruses with the mutated S proteins to BNT162b2-induced antisera. As shown in Figure 2H, the G75V, T76I, GT75-76VI, and T859N mutations did not affect vaccine-induced neutralization. In contrast, the RSYLTPGD246-253N mutant exhibited significant resistance to the vaccine-induced neutralization (Figure 2H: $p = 0.027$ by the Wilcoxon matched-pairs signed rank test), which is relevant to the experiment with the S proteins of the Lambda variant and the Lambda + N246-253RSYLTPGD derivative (Figure 2B). In addition, we found that the L452Q and F490S mutations confer resistance to vaccine-induced antisera (Figure 2H). The finding that the F490S mutation does not affect viral infectivity (Figure 2E) but confers the resistance to the vaccine-induced antisera (Figure 2H) suggests that this mutant has acquired resistance to antiviral humoral immunity. In contrast, the L452Q mutation not only increases viral infectivity (Figure 2E) and affinity to ACE2 (Figure 2F) but also augments resistance to the vaccine-induced antiviral cellular (Figure 2G) and humoral immunities (Figure 2H), suggesting that this mutation is critical for the viral dissemination in the human population.

### Effects of NTD-targeting monoclonal antibodies on Lambda variant infection

To further assess the effect of the mutations in Lambda S, particularly those in the NTD, we used 2 monoclonal antibodies that target the NTD: an NTD-targeting NAb, clone 4A8 (Chi et al., 2020), and an EAb, clone COV2-2490, that recognizes the NTD and enhances viral infectivity (Liu et al., 2021c). As shown in Figures 2I and 2J, the 4A8 antibody detected the cell surface expression of S proteins of the parental virus, Lambda + N246-253RSYLTPGD derivative, G75V, T76I, and GT75-76VI and inhibited the infections of these pseudoviruses in a dose-dependent manner. Intriguingly, the 4A8 antibody failed to detect the surface expression of the S proteins of the Lambda and the RSYLTPGD246-253N mutant (Figure 2I), and the pseudoviruses with the S proteins of the Lambda and the RSYLTPGD246-253N mutant were resistant to the antiviral effect mediated by the 4A8 antibody (Figure 2J). Because a polyclonal antibody targeting the SARS-CoV-2 S protein detected these mutants, similar to the parental S (Figure S2I), our results suggest that the RSYLTPGD246-253N mutation critically affects the sensitivity to certain NAbs targeting the NTD, such as the 4A8 antibody.

For the COV2-2490 antibody, flow cytometry analysis showed that this antibody more efficiently detects the Lambda S than the parental S (Figure 2K). Although this antibody enhanced the infectivities of all of the pseudoviruses tested (Figure 2L), it is important to note that the infectivity of the Lambda S was more significantly enhanced than that of the parental S (Figure 2L: $p = 0.032$ at 0.010 $\mu$g/mL; $p = 0.013$ at 0.1 $\mu$g/mL; $p = 0.024$ at 1.0 $\mu$g/mL by Student's t test). These data suggest that Lambda S is more susceptible to EAb-mediated enhancement of viral infection. Because an apparent enhancement of viral infectivity compared to the parental S pseudovirus was not observed in the substituted mutants (G75V, T76I, GT75-76VI, and RSYLTPGD246-253N) (Figure 2L), our data suggest that multiple mutations in the NTD of Lambda S are crucial for the augmented enhancement of viral infectivity. Although the surface detection level of the Lambda variant was comparable to those of the Lambda + N246-253RSYLTPGD derivative and other NTD mutants tested (T76I, GT75-76VI, and RSYLTPGD246-253N) (Figure 2K), the augmented enhancement of viral infectivity was specific for the Lambda S (Figure 2L). These observations suggest that the detection level of the S protein on the cell surface by flow cytometry does not necessarily reflect the augmentation level of viral infection by the COV2-2490 antibody, and further actions of the S protein following the binding of the COV2-2490 antibody, such as the Lambda S-specific conformational change, may be needed to lead to the augmented enhancement of viral infectivity.

### Association of a nascent N-linked glycosylation site (NLGS) by the RSYLTPGD246-253N mutation with sensitivity to NTD-targeting antibodies

We revealed that Lambda S is more resistant to vaccine-induced antiviral humoral immunity (Figures 2B and 2H) as well as an NTD-targeting NAb (Figure 2J) and that the RSYLTPGD246-253N mutation is responsible for NAb resistance. In addition, the sensitivity of Lambda S to EAb was higher than that of the parental S and was also attributed

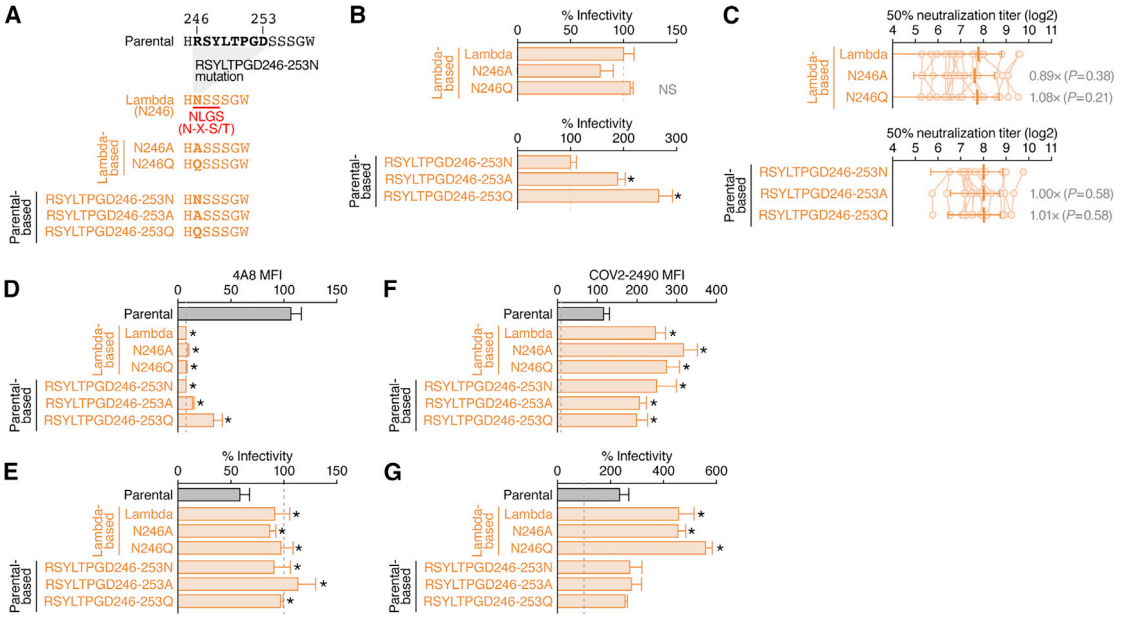


**Figure 3. Effect of the nascent NLGS by the RSYLTPGD246-253N mutation on sensitivity to antibodies**

(A) A scheme showing the generation of the NLGS by the RSYLTPGD246-253N mutation. The NLGS generated in the Lambda S is indicated in red.

(B) Pseudovirus assay. HIV-1-based reporter viruses pseudotyped with SARS-CoV-2 S proteins bearing mutations based on the Lambda S (top) and the parental S RSYLTPGD246-253N mutant (bottom) were prepared. The pseudoviruses were inoculated in HOS-ACE2/TMPRSS2 cells at 1,000 ng HIV-1 p24 antigen, and the percentages of infectivity compared to that of the virus pseudotyped with parental S are shown.

(C) Neutralization assay. A neutralization assay was performed using pseudoviruses with SARS-CoV-2 S proteins bearing respective mutations based on the Lambda S and the parental S RSYLTPGD246-253N mutant and 18 BNT162b2-vaccinated sera (same as those used in Figure 2B), as described in STAR Methods. The number in the panel indicates the fold change in neutralization resistance of the pseudoviruses, with the mutations indicated to those with respective parental S.

(D–G) Effect of monoclonal antibodies. The MFI of the surface S proteins stained with NTD-targeting NAb clone 4A8 (151 ng/mL) (Chi et al., 2020) (D) and EAb clone COV2-2490 (1 μg/mL) (Liu et al., 2021c) (F) antibodies. (E) Antiviral effect of the NTD-targeting NAb clone 4A8 antibody. (G) Enhancing effect of the EAb clone COV2-2490 antibody. The percentages of infectivity compared to that of the virus without antibodies are shown.

Assays were performed in triplicate, and the mean is shown with the SD.

In (B), statistically significant differences (*p < 0.05) versus the Lambda S (top) or the parental S RSYLTPGD246-253N mutant (bottom) were determined by Student's t test.

In (B), (E), and (G), vertical dashed lines indicate 100% (the value of Lambda S [A, top], parental S RSYLTPGD246-253N mutant [A, bottom], or parental S [E and G]).

In (C), statistically significant differences were determined by the Wilcoxon matched-pairs signed rank test. The p values are indicated in the figure.

In (D)–(G), statistically significant differences (*p < 0.05) versus parental S were determined by Student's t test.

In (D) and (F), vertical dashed lines indicate the MFIs of mock-transfected cells.

NS, no statistical significance.

to the multiple mutations in the NTD, including the RSYLTPGD246-253N mutation (Figure 2L). These data suggest the importance of the RSYLTPGD246-253N mutation in determining the virological phenotype of Lambda S; however, it remains unclear how this large mutation affects sensitivity to neutralizing/enhancing antibodies. When we further assessed the amino acid sequences of the S proteins of the parental and Lambda variant, we found that the RSYLTPGD246-253N mutation generates an NLGS (N-X-S/T consensus sequence) *de novo* (Figure 3A). Because emergent N-linked glycans in viral spike proteins, such as HIV-1 envelope protein (Li et al., 2008; Quinones-Kochs et al., 2002; Reitter et al., 1998; Wagh et al., 2020), and influenza A virus hemagglutinin protein (Abe et al., 2004; Kobayashi and Suzuki, 2012; Skehel et al., 1984; Wang et al., 2009), can shield the viral particles from NAbs, we hypothesized that this property of Lambda S is attributed to the nascent N-glycan conferred by the RSYLTPGD246-253N mutation. To address this possibility, we prepared two Lambda S derivatives, N246A and N246Q, which abolished the NLGS (Figure 3A). We also prepared two parental S RSYLTPGD246-253N mutant-based derivatives, RSYLTPGD246-253A and RSYLTPGD246-253Q (Figure 3A). As shown in Figure 3B, the infectivities of the parental S RSYLTPGD246-253N mutant-based pseudoviruses ($p < 0.0001$, RSYLTPGD246-253A versus parental; $p < 0.0001$, RSYLTPGD246-253Q versus parental by Student's t test) but not that of the Lambda S-based pseudoviruses ($p = 0.081$, RSYLTPGD246-253A versus Lambda; $p = 0.26$, RSYLTPGD246-253Q versus Lambda by Student's t test) were significantly increased by the NLGS disruption. However, NLGS disruption did not affect the sensitivity to vaccine-induced NAbs (Figure 3C). As in the cases of the Lambda S

and the parental S RSYLTPGD246-253N mutant (Figure 2I), flow cytometry analysis showed that the 4A8 antibody faintly detected the NLGS-disrupted mutants on the cell surface (Figure 3D). In addition, a neutralization assay revealed that the NLGS disruption did not affect the sensitivity to the 4A8 antibody (Figure 3E). For an NTD-targeting EAb, the COV2-2490 antibody, the detection on the cell surface by flow cytometry (Figure 3F), and the enhancement of the pseudovirus infectivity (Figure 3G) were comparable between the NLGS-disrupted mutants and the Lambda S and the parental S RSYLTPGD246-253N mutants. These results suggest that the addition of an NLGS does not affect the sensitivity of Lambda S to the antibodies targeting the NTD.

## DISCUSSION

In this study, we demonstrated that 3 mutations, the RSYLTPGD246-253N, L452Q, and F490S mutations, confer resistance to vaccine-induced antiviral humoral immunity. In addition, the L452Q mutation allows evasion of HLA-A24-restricted cellular immunity. Moreover, the T76I and L452Q mutations contribute to enhanced viral infectivity. Our investigations using pseudoviruses suggest at least 2 virological features of the S protein of the Lambda variant: increasing viral infectivity (by the T76I and L452Q mutations) and exhibiting resistance to antiviral immunity (by the RSYLTPGD246-253N, L452Q, and F490S mutations).

Molecular phylogenetic analyses showed that the acquisition of a 7-amino acid deletion, the RSYLTPGD246-253N mutation, in the Lambda variant is closely associated with the increase in the effective population size of this variant. Here, we demonstrated that the RSYLTPGD246-253N mutation does not affect viral infectivity, but is responsible for resistance to vaccine-induced neutralization as well as an NTD-targeting NAb (4A8). Although the RSYLTPGD246-253N mutation generates a nascent NLGS, the addition of N-linked glycan did not affect NAb resistance in our assays. Notably, the RSYLTPGD246-253N mutation overlaps with a component of the NTD "supersite" (Chi et al., 2020). Our results suggest that the 7-amino acid deletion rather than the addition of the asparagine residue leading to the formation of a new NLGS confers NAb resistance and further supports the possibility that the NTD supersite is immunodominant and the mutations in this site are closely associated with the efficacy of vaccine-induced neutralization.

It has been reported that the SARS-CoV-2 S forms some conformational patterns, and the opened RBD state exposes the ACE2 binding interface (Li et al., 2020; Plante et al., 2021; Yurkovetskiy et al., 2020). Also, Liu et al. (2021c) revealed that the binding of EAbs, including COV2-2490, to the SARS-CoV-2 S NTD induces the conformation of the opened RBD state leading to enhanced binding to ACE2. Here, we demonstrated that multiple mutations in the NTD, including the RSYLTPGD246-253N mutation, contribute to the augmented enhancement of viral infection by an EAb (COV2-2490). Because the epitope of COV2-2490 does not overlap the mutations in the NTD of Lambda S (G75V, T76I, and RSYLTPGD246-253N) (Liu et al., 2021c), these mutations would not directly affect the binding affinity of this antibody to S. Rather, these mutations may indirectly increase the affinity of this antibody to S through the conformational change of NTD overall. Our results suggest that the emergence of the RSYLTPGD246-253N mutation was a driving force of the spread of this variant in the human population, possibly due to the acquisition of 2 antibody-associated properties, resistance to NAbs and enhanced benefits from EAbs.

We showed that the infectivity of the viruses pseudotyped with the Lambda S is significantly higher than that of the parental S. In addition, consistent with our previous reports (Mlcochova et al., 2021; Motozono et al., 2021), the infectivity of the viruses pseudotyped with the S proteins of the Delta and Epsilon variants was significantly higher than that of the parental S. A common feature of the Lambda, Delta, and Epsilon variants is a substitution in L452 of the SARS-CoV-2 S protein: the Lambda variant harbors the L452Q mutation, while the Delta and Epsilon variants possess the L452R mutation (Mlcochova et al., 2021; Motozono et al., 2021). Here, we demonstrated that the L452Q mutation increases viral infectivity. Together with our previous observation that the L452R mutation enhances viral infectivity (Motozono et al., 2021), these results strongly suggest that the relatively higher infectivity of the Lambda, Delta, and Epsilon variants is attributed to the L452Q/R mutation. The fact that the Lambda and Delta variants are currently a VOI and a VOC, respectively, suggests that their increasing spread in the human population is partly attributed to their higher infectivity than that of the parental SARS-CoV-2. In contrast, despite its higher infectivity, the Epsilon variant, an ex-VOC, was excluded from the VOC/VOI classification on July 6, 2021 because this variant was stamped out (WHO, 2021a). The transient and unsuccessful (compared to the other VOCs) spread of the Epsilon variant in the human population implies that increasing viral infectivity is insufficient to maintain efficient spread in the human population. In addition to increased viral infectivity, the Delta variant exhibits higher resistance to vaccine-induced neutralization (Mlcochova et al., 2021; Wall et al., 2021). Similarly, here, we showed that the Lambda variant shows increased infectivity and resistance against antiviral immunity. These observations suggest that acquiring at least two virological features, increased viral infectivity and evasion from antiviral immunity, is pivotal for efficient spread and transmission in the human population.

We showed that the Lambda S is more resistant to the vaccine sera than the parental S (Figure 2B). By the loss-of-function experiment, we also showed that this immune resistance was canceled by the reversion of the NTD deletion (RSYLTPGD246-253N mutation) in the context of the Lambda variant (Figure 2B), suggesting that the immune resistance of Lambda variant is mostly dependent primarily on the RSYLTPGD246-253N mutation located in NTD. However, in the gain-of-function experiment based on the parental S (Figure 2H), the 3 mutations detected in the Lambda variant, RSYLTPGD246-253N, L452Q, and F490S, can lead to the resistance to vaccine sera. The discrepancy between these 2 experiments can be explained by the context of S proteins used as the backbone. The gain-of-function experiment (Figure 2H) suggests the potential of the RSYLTPGD246-253N, L452Q, and F490S mutations to confer resistance to vaccine sera, when the backbone is parental S protein. However, the loss-of-function experiment (Figure 2B) suggests that the RSYLTPGD246-253N mutation determines the resistance to

vaccine sera, when the backbone is the Lambda S. Because the Lambda S contains the other mutations compared to the parental S, our data suggest that the resistance to the vaccine sera (i.e., polyclonal antibodies elicited by vaccination) is dependent on the context of S protein sequence and/or structure. Similarly, the context-dependent effect by the mutation insertion was also observed in the pseudovirus infection assay (Figure 3B); the RSYLTPGD246-253A/Q mutation increased the infectivity of the parental RSYLTPGD246-253N-based S but did not increase that of the Lambda S. Our findings suggest that the effects of mutations on viral infectivity and immune resistance should be carefully evaluated based on the context of S protein used as the backbone.

In addition to the aforementioned virological property of the Lambda S via the mutations in its NTD, we revealed that a mutation in its RBD, L452Q, confers 2 virological properties: increase in viral infectivity and evasion from the HLA-A24-restricted cellular immunity. These are reminiscent of our recent study showing that the L452R mutation confers similar virological phenotypes (Motozono et al., 2021). In particular, regarding the latter phenotype, it is possible that the immune pressure elicited by the HLA-A24$^{+}$ individuals living in South American countries, where the Lambda variant mainly spreads, was the driving force in the emergence of this mutation. In fact, the allele frequencies of HLA-A24 in the populations of South American countries such as Peru, Chile, and Argentina, where the Lambda variant has been widespread (Figure 1A), were 9.1%, 11.1%, and 10.7% for people in Peru (n = 251), Chile (n = 920), and Argentina (n = 2,516), respectively (Gonzalez-Galarza et al., 2020). Assuming that the Hardy-Weinberg law is valid, the frequencies of the people who have at least 1 HLA-A24 allele are 17.5% (Peru), 21.0% (Chile), and 20.2% (Argentina), respectively, which are relatively higher numbers considering the diversity of HLA alleles. Therefore, it would be reasonable to assume that the L452Q mutation that emerged via the HLA-A24-mediated immune pressure and the acquisition of this mutation to evade HLA-A24-mediated cellular immunity may further contribute to the relatively higher prevalence of the Lambda variant in these countries.

Gobeil et al., 2021 suggested that mutations in the S NTD drive viral transmission and escape from antiviral immunity. In fact, three of the current four VOCs harbor deletions in the S NTD (reviewed in Harvey et al. [2021]). The Alpha variant has a 2-amino acid deletion, the HV69-70 deletion, in the NTD. Meng et al. (2021) showed that the HV69-70 deletion does not affect NAb sensitivity but does increase viral infectivity, suggesting that the virological importance of the deletion of a portion of the NTD between the Alpha (the HV69-70 deletion) and the Lambda variants (the RSYLTPGD246-253N mutation) is different. A cluster of the Beta variant also possesses a 3-amino acid deletion, the LAL242-244 deletion. This deletion does not critically affect sensitivity to vaccine-induced neutralization but results in resistance to some NTD-targeting NAbs, such as 4A8 (Liu et al., 2021b; Wang et al., 2021b). Interestingly, the Delta variant (B.1.617.2 lineage), a VOC, harbors a 2-amino acid deletion, the EFR156-158G mutation, while its relative VOI, the Kappa variant (B.1.617.1 lineage), does not (WHO, 2021a). Although the virological importance of the EFR156-158G mutation remains unclear, this mutation in the S NTD may be associated with the spread of the Delta variant worldwide. Together with our findings that RSYLTPGD246-253N confers resistance to vaccine-induced antisera and an NTD-targeting NAb, 4A8, the accumulating mutations in the S NTD may be closely associated with the virological features of the variants that can explain their spreading efficacy in the human population. In particular, 4A8 targets the NTD supersite (Harvey et al., 2021; Lok, 2021) that includes RSYLTPGD246-253 (Chi et al., 2020). Because the RSYLTPGD246-253N mutation is responsible for the resistance to the vaccine-induced antiviral effect of the Lambda variant, our data indicate that the NTD supersite is immunodominant and that acquiring immune escape mutations in this region is associated with the efficacy of viral dissemination in the human population, which has been proposed in previous reports (Harvey et al., 2021; McCallum et al., 2021). Moreover, we revealed that an EAb, COV2-2490, preferentially enhances Lambda S-mediated infection. Although this enhancing effect is not specifically attributed to the RSYLTPGD246-253N mutation, such enhancement may be associated with the potential spread of the Lambda variant.

Through molecular phylogenetic analyses and virological experiments, we elucidated how the Lambda variant originated and acquired its virological properties. Because the Lambda variant is a VOI, it may be believed that this variant is not an ongoing threat compared to pandemic VOCs. However, because the Lambda variant is relatively resistant to vaccine-induced antisera, this variant may cause breakthrough infections (Hacisuleyman et al., 2021; Jacobson et al., 2021; Nixon and Ndhlovu, 2021; Rana et al., 2021). Moreover, elucidating the evolutionary traits of threatening SARS-CoV-2 variants can help predict the possibility of a wider epidemic, and revealing the virological features of the respective mutations in VOCs and VOIs is essential to assess the risk of newly emerging SARS-CoV-2 variants in the future.

## Limitations of the study

The experiments using pseudoviruses showed that the Lambda variant is more infectious than the parental virus (Figure 2A). However, it remains unaddressed whether the live SARS-CoV-2 Lambda variant is more replicative than the live parental SARS-CoV-2 (B.1 lineage). Although our data showed that the Alpha pseudovirus is less infectious than the parental (B.1 lineage) pseudovirus, which is consistent with a previous study (Acevedo et al., 2021), Touret et al. (2021) showed that the growth capacity of the live Alpha variant is comparable to that of the B.1 lineage virus. Because the cells used for the infection experiments are different, the discrepancy between the pseudovirus assay and the experiment using live virus may be due to the differences in the experimental setup. Further investigation will be needed to evaluate the replication capacity of SARS-CoV-2 variants using live viruses and multiple cell types. However, the use of live SARS-CoV-2 variants for in-depth experiments is still limited by experimental, processing, and safety limitations.

Consistent with a previous report (Liu et al., 2021c), we showed that an EAb, COV2-2490, enhanced viral infectivity in *in vitro* cell culture experiments (Figures 2L and 3G). In addition, COV2-2490 confers greater benefit to the Lambda pseudovirus

(Figures 2L and 3G). However, Li et al. (2021) reported that the EAbs do not necessarily promote viral expansion in an *in vivo* animal model. Because the effect of EAbs on viral replication *in vitro* and *in vivo* may be inconsistent, the possibility of the contribution of EAbs for the expansion of Lambda variant as well as other VOCs/VOCs *in vivo* should be addressed in the future.

## STAR★METHODS

Detailed methods are provided in the online version of this paper and include the following:

- KEY RESOURCES TABLE
- RESOURCE AVAILABILITY
  - Lead contact
  - Materials availability
  - Data and code availability
- EXPERIMENTAL MODEL AND SUBJECT DETAILS
  - Ethics statement
  - Collection of sera from BNT162b2-Vaccinated individuals
  - Collection of human PBMCs
  - Cell culture
- METHOD DETAILS
  - Viral genome sequence analysis
  - Protein structure homology model
  - Plasmid construction
  - Pseudovirus assay
  - Antibody treatment
  - Yeast surface display
  - Activation-induced marker assay
  - Intracellular cytokine staining
  - Flow cytometry
- QUANTIFICATION AND STATISTICAL ANALYSIS

## SUPPLEMENTAL INFORMATION

Supplemental information can be found online at https://doi.org/10.1016/j.celrep.2021.110218.

## CONSORTIA

The Genotype to Phenotype Japan (G2P-Japan) Consortium: Mika Chiba, Shigeru Fujita, Hirotake Furihata, Naoko Misawa, Nanami Morizako, Akiko Oide, Seiya Ozono, Mai Suganami, Miyoko Takahashi, Mako Toyoda, and Miyabishara Yokoyama.

## ACKNOWLEDGMENTS

We would like to thank all of the members belonging to The Genotype to Phenotype Japan (G2P-Japan) Consortium. The supercomputing resource was provided by Human Genome Center at the University of Tokyo and the NIG supercomputer at ROIS National Institute of Genetics. We thank Dr. Masafumi Takiguchi (Kumamoto University, Japan) for providing C1R-A2402 cells. This study was supported in part by the AMED Research Program on Emerging and Re-emerging Infectious Diseases 20fk0108539 (to T.U.), 20fk0108542 and 20fk0108403 (to H.A.), 20fk0108163 and 20fk0108518 (to A.S.), 20fk0108146 and 20fk0108270 (to K. Sato), 20fk0108413 (to S.N. and K. Sato), and 20fk0108451 (to G2P-Japan Consortium, T.U., A.T.-K., A.S., S.N. and K. Sato); the AMED Research Program on HIV/AIDS 21fk0410046 (to C.M.), 21fk0410033 (to A.S.), and 21fk0410039 (to K. Sato); the AMED Japan Program for Infectious Diseases Research and Infrastructure 20wm0325009 and 21wm0325009 (to A.S.); JST SICORP (e-ASIA) JPMJSC20U1 (to K. Sato); JST SICORP JPMJSC21U5 (to K.Sato); JST CREST JPMJCR20H6 (to S.N.) and JPMJCR20H4 (to K. Sato); JSPS KAKENHI Grant-in-Aid for Scientific Research C 18K07156 and 21K07060 (to K.T.), Scientific Research S 18H05279 (to H.A.), Scientific Research C 19K06382 (to A.S.), and Scientific Research B 18H02662 (to K. Sato) and 21H02737 (to K. Sato); the JSPS Fund for the Promotion of Joint International Research (Fostering Joint International Research) 18KK0447 (to K. Sato); the JSPS Core-to-Core Program JPJSCCA20190008 (A. Advanced Research Networks) (to K. Sato); the JSPS Research Fellow DC1 19J20488 (to I.K.); the Ono Medical Research Foundation (to K. Sato); the Ichiro Kanehara Foundation (to K. Sato); the Lotte Foundation (to K. Sato); the Mochida Memorial Foundation for Medical and Pharmaceutical Research (to K. Sato); the Daiichi Sankyo Foundation of Life Science (to K. Sato); the Sumitomo Foundation (to K. Sato); the Uehara Foundation (to K. Sato); the Takeda Science Foundation (to C.M. and K. Sato); The Tokyo Biochemical Research Foundation (to K. Sato); a Grant for Joint Research Projects of the Research Institute for Microbial Diseases, Osaka University (to A.S.); an intramural grant from Kumamoto University COVID-19 Research Projects (AMABIE) (to C.M.); and the Joint Usage/Research Center Program of Institute for Frontier Life and Medical Sciences, Kyoto University (to K. Sato).

## AUTHOR CONTRIBUTIONS

I.K., Y. Kosugi, J.Z., D.Y., E.P.B., Y.L.T., K.U., N.M., C.M., A.S., and K. Sato performed the experiments. K. Shirakawa, Y. Kazuma, R.N., Y.H., and A.T.-K. collected the clinical samples. Y.L. and H.A. prepared the reagents. I.K., Y. Kosugi, J.Z., D.Y., E.P.B., Y.L.T., K.U., K.T., T.U., G.S., C.M., A.S., and K. Sato designed the experiments and interpreted the results. J.W. and S.N. performed the molecular phylogenetic analysis. K. Sato wrote the original manuscript. All of the authors reviewed and proofread the manuscript. The Genotype to Phenotype Japan (G2P-Japan) Consortium contributed to the project administration.

## DECLARATION OF INTERESTS

The authors declare no competing interests.

Received: August 30, 2021
Revised: November 24, 2021
Accepted: December 14, 2021
Published: December 18, 2021

## REFERENCES

Abe, Y., Takashita, E., Sugawara, K., Matsuzaki, Y., Muraki, Y., and Hongo, S. (2004). Effect of the addition of oligosaccharides on the biological activities and antigenicity of influenza A/H3N2 virus hemagglutinin. J. Virol. *78*, 9605–9611.

Acevedo, M.L., Alonso-Palomares, L., Bustamante, A., Gaggero, A., Paredes, F., Cortés, C.P., Valiente-Echeverría, F., and Soto-Rifo, R. (2021). Infectivity and immune escape of the new SARS-CoV-2 variant of interest Lambda. MedRxiv, 21259673.

Chen, R.E., Zhang, X., Case, J.B., Winkler, E.S., Liu, Y., VanBlargan, L.A., Liu, J., Errico, J.M., Xie, X., Suryadevara, N., et al. (2021). Resistance of SARS-CoV-2 variants to neutralization by monoclonal and serum-derived polyclonal antibodies. Nat. Med. *27*, 717–726.

Chi, X., Yan, R., Zhang, J., Zhang, G., Zhang, Y., Hao, M., Zhang, Z., Fan, P., Dong, Y., Yang, Y., et al. (2020). A neutralizing human antibody binds to the N-terminal domain of the Spike protein of SARS-CoV-2. Science *369*, 650–655.

Collier, D.A., De Marco, A., Ferreira, I., Meng, B., Datir, R., Walls, A.C., Kemp, S.S., Bassi, J., Pinto, D., Fregni, C.S., et al. (2021). Sensitivity of SARS-CoV-2 B.1.1.7 to mRNA vaccine-elicited antibodies. Nature *593*, 136–141.

Ferreira, I., Kemp, S.A., Datir, R., Saito, A., Meng, B., Rakshit, P., Takaori-Kondo, A., Kosugi, Y., Uriu, K., Kimura, I., et al. (2021). SARS-CoV-2 B.1.617

mutations L452R and E484Q are not synergistic for antibody evasion. J. Infect. Dis. *224*, 989–994.

Fiser, A., Do, R.K., and Sali, A. (2000). Modeling of loops in protein structures. Protein Sci. *9*, 1753–1773.

Gao, A., Chen, Z., Amitai, A., Doelger, J., Mallajosyula, V., Sundquist, E., Segal, F.P., Carrington, M., Davis, M.M., Streeck, H., et al. (2021). Learning from HIV-1 to predict the immunogenicity of T cell epitopes in SARS-COV-2. iScience, 102311.

Garcia-Beltran, W.F., Lam, E.C., St Denis, K., Nitido, A.D., Garcia, Z.H., Hauser, B.M., Feldman, J., Pavlovic, M.N., Gregory, D.J., Poznansky, M.C., et al. (2021). Multiple SARS-CoV-2 variants escape neutralization by vaccine-induced humoral immunity. Cell *184*, 2372–2383.e9.

Gobeil, S.M., Janowska, K., McDowell, S., Mansouri, K., Parks, R., Stalls, V., Kopp, M.F., Manne, K., Li, D., Wiehe, K., et al. (2021). Effect of natural mutations of SARS-CoV-2 on spike structure, conformation, and antigenicity. Science *373*, 1353–1360.

Gonzalez-Galarza, F.F., McCabe, A., Santos, E., Jones, J., Takeshita, L., Ortega-Rivera, N.D., Cid-Pavon, G.M.D., Ramsbottom, K., Ghattaoraya, G., Alfirevic, A., et al. (2020). Allele frequency net database (AFND) 2020 update: gold-standard data classification, open access genotype data and new query tools. Nucleic Acids Res. *48*, D783–D788.

Hacisuleyman, E., Hale, C., Saito, Y., Blachere, N.E., Bergh, M., Conlon, E.G., Schaefer-Babajew, D.J., DaSilva, J., Muecksch, F., Gaebler, C., et al. (2021). Vaccine breakthrough infections with SARS-CoV-2 variants. N. Engl. J. Med. *384*, 2212–2218.

Harvey, W.T., Carabelli, A.M., Jackson, B., Gupta, R.K., Thomson, E.C., Harrison, E.M., Ludden, C., Reeve, R., Rambaut, A., Consortium, C.-G.U., et al. (2021). SARS-CoV-2 variants, spike mutations and immune escape. Nat. Rev. Microbiol. *19*, 409–424.

Hoffmann, M., Arora, P., Gross, R., Seidel, A., Hornich, B.F., Hahn, A.S., Kruger, N., Graichen, L., Hofmann-Winkler, H., Kempf, A., et al. (2021). SARS-CoV-2 variants B.1.351 and P.1 escape from neutralizing antibodies. Cell *184*, 2384–2393.e12.

Hu, C., Shen, M., Han, X., Chen, Q., Li, L., Chen, S., Zhang, J., Gao, F., Wang, W., Wang, Y., et al. (2021). Identification of cross-reactive CD8$^+$ T cell receptors with high functional avidity to a SARS-CoV-2 immunodominant epitope and its natural mutant variants. Genes Dis. *9*, 216–229.

Jackson, B., Boni, M.F., Bull, M.J., Colleran, A., Colquhoun, R.M., Darby, A., Haldenby, S., Hill, V., Lucaci, A., McCrone, J.T., et al. (2021). Generation and transmission of interlineage recombinants in the SARS-CoV-2 pandemic. Cell *184*, 5179–5188.e8.

Jacobson, K.B., Pinsky, B.A., Montez Rath, M.E., Wang, H., Miller, J.A., Skhiri, M., Shepard, J., Mathew, R., Lee, G., Bohman, B., et al. (2021). Post-vaccination SARS-CoV-2 infections and incidence of presumptive B.1.427/B.1.429 variant among healthcare personnel at a northern California academic medical center. Clin. Infect. Dis.ciab554 https://doi.org/10.1093/cid/ciab554.

Jara, A., Undurraga, E.A., Gonzalez, C., Paredes, F., Fontecilla, T., Jara, G., Pizarro, A., Acevedo, J., Leo, K., Leon, F., et al. (2021). Effectiveness of an inactivated SARS-CoV-2 vaccine in Chile. N. Engl. J. Med. *385*, 946–948.

Karaki, S., Kariyone, A., Kato, N., Kano, K., Iwakura, Y., and Takiguchi, M. (1993). HLA-B51 transgenic mice as recipients for production of polymorphic HLA-A, B-specific antibodies. Immunogenetics *37*, 139–142.

Kared, H., Redd, A.D., Bloch, E.M., Bonny, T.S., Sumatoh, H., Kairi, F., Carbajo, D., Abel, B., Newell, E.W., Bettinotti, M.P., et al. (2021). SARS-CoV-2-specific CD8$^+$ T cell responses in convalescent COVID-19 individuals. J. Clin. Invest. *131*, e145476.

Katoh, K., and Standley, D.M. (2013). MAFFT multiple sequence alignment software version 7: improvements in performance and usability. Mol. Biol. Evol. *30*, 772–780.

Kobayashi, Y., and Suzuki, Y. (2012). Evidence for N-glycan shielding of antigenic sites during evolution of human influenza A virus hemagglutinin. J. Virol. *86*, 3446–3451.

Li, D., Edwards, R.J., Manne, K., Martinez, D.R., Schafer, A., Alam, S.M., Wiehe, K., Lu, X., Parks, R., Sutherland, L.L., et al. (2021). *In vitro* and *in vivo* functions of SARS-CoV-2 infection-enhancing and neutralizing antibodies. Cell *184*, 4203–4219.e32.

Li, Q., Wu, J., Nie, J., Zhang, L., Hao, H., Liu, S., Zhao, C., Zhang, Q., Liu, H., Nie, L., et al. (2020). The impact of mutations in SARS-CoV-2 spike on viral infectivity and antigenicity. Cell *182*, 1284–1294 e9.

Li, Y., Cleveland, B., Klots, I., Travis, B., Richardson, B.A., Anderson, D., Montefiori, D., Polacino, P., and Hu, S.L. (2008). Removal of a single N-linked glycan in human immunodeficiency virus type 1 gp120 results in an enhanced ability to induce neutralizing antibody responses. J. Virol. *82*, 638–651.

Liu, J., Liu, Y., Xia, H., Zou, J., Weaver, S.C., Swanson, K.A., Cai, H., Cutler, M., Cooper, D., Muik, A., et al. (2021a). BNT162b2-elicited neutralization of B.1.617 and other SARS-CoV-2 variants. Nature *596*, 273–275.

Liu, Y., Liu, J., Xia, H., Zhang, X., Fontes-Garfias, C.R., Swanson, K.A., Cai, H., Sarkar, R., Chen, W., Cutler, M., et al. (2021b). Neutralizing activity of BNT162b2-elicited serum. N. Engl. J. Med. *384*, 1466–1468.

Liu, Y., Soh, W.T., Kishikawa, J.I., Hirose, M., Nakayama, E.E., Li, S., Sasai, M., Suzuki, T., Tada, A., Arakawa, A., et al. (2021c). An infectivity-enhancing site on the SARS-CoV-2 spike protein targeted by antibodies. Cell *184*, 3452–3466 e3418.

Lok, S.M. (2021). An NTD supersite of attack. Cell Host Microbe. *29*, 744–746.

McCallum, M., De Marco, A., Lempp, F.A., Tortorici, M.A., Pinto, D., Walls, A.C., Beltramello, M., Chen, A., Liu, Z., Zatta, F., et al. (2021). N-terminal domain antigenic mapping reveals a site of vulnerability for SARS-CoV-2. Cell *184*, 2332–2347.e6.

Meng, B., Kemp, S.A., Papa, G., Datir, R., Ferreira, I., Marelli, S., Harvey, W.T., Lytras, S., Mohamed, A., Gallo, G., et al. (2021). Recurrent emergence of SARS-CoV-2 spike deletion H69/V70 and its role in the Alpha variant B.1.1.7. Cell Rep. *35*, 109292.

Minh, B.Q., Schmidt, H.A., Chernomor, O., Schrempf, D., Woodhams, M.D., von Haeseler, A., and Lanfear, R. (2020). IQ-TREE 2: new models and efficient methods for phylogenetic inference in the genomic era. Mol. Biol. Evol. *37*, 1530–1534.

MIcochova, P., Kemp, S.A., Dhar, M.S., Papa, G., Meng, B., Ferreira, I., Datir, R., Collier, D.A., Albecka, A., Singh, S., et al. (2021). SARS-CoV-2 B.1.617.2 Delta variant replication and immune evasion. Nature *599*, 114–119.

Motozono, C., Toyoda, M., Zahradnik, J., Saito, A., Nasser, H., Tan, T.S., Ngare, I., Kimura, I., Uriu, K., Kosugi, Y., et al. (2021). SARS-CoV-2 spike L452R variant evades cellular immunity and increases infectivity. Cell Host Microbe. *29*, 1124–1136.

Niwa, H., Yamamura, K., and Miyazaki, J. (1991). Efficient selection for high-expression transfectants with a novel eukaryotic vector. Gene *108*, 193–199.

Nixon, D.F., and Ndhlovu, L.C. (2021). Vaccine breakthrough infections with SARS-CoV-2 variants. N. Engl. J. Med. *385*, e7.

Ozono, S., Zhang, Y., Ode, H., Sano, K., Tan, T.S., Imai, K., Miyoshi, K., Kishigami, S., Ueno, T., Iwatani, Y., et al. (2021). SARS-CoV-2 D614G spike mutation increases entry efficiency with enhanced ACE2-binding affinity. Nat. Commun. *12*, 848.

Ozono, S., Zhang, Y., Tobiume, M., Kishigami, S., and Tokunaga, K. (2020). Super-rapid quantitation of the production of HIV-1 harboring a luminescent peptide tag. J. Biol. Chem. *295*, 13023–13030.

Peleg, Y., and Unger, T. (2014). Application of the restriction-free (RF) cloning for multicomponents assembly. Methods Mol. Biol. *1116*, 73–87.

Piccoli, L., Park, Y.J., Tortorici, M.A., Czudnochowski, N., Walls, A.C., Beltramello, M., Silacci-Fregni, C., Pinto, D., Rosen, L.E., Bowen, J.E., et al. (2020). Mapping neutralizing and immunodominant sites on the SARS-CoV-2 spike receptor-binding domain by structure-guided high-resolution serology. Cell *183*, 1024–1042 e1.

Planas, D., Bruel, T., Grzelak, L., Guivel-Benhassine, F., Staropoli, I., Porrot, F., Planchais, C., Buchrieser, J., Rajah, M.M., Bishop, E., et al. (2021). Sensitivity of infectious SARS-CoV-2 B.1.1.7 and B.1.351 variants to neutralizing antibodies. Nat. Med. *27*, 917–924.

Plante, J.A., Liu, Y., Liu, J., Xia, H., Johnson, B.A., Lokugamage, K.G., Zhang, X., Muruato, A.E., Zou, J., Fontes-Garfias, C.R., et al. (2021). Spike mutation D614G alters SARS-CoV-2 fitness. Nature *592*, 116–121.

Quinones-Kochs, M.I., Buonocore, L., and Rose, J.K. (2002). Role of N-linked glycans in a human immunodeficiency virus envelope glycoprotein: effects on protein function and the neutralizing antibody response. J. Virol. *76*, 4199–4211.

Rambaut, A., Holmes, E.C., O'Toole, A., Hill, V., McCrone, J.T., Ruis, C., du Plessis, L., and Pybus, O.G. (2020). A dynamic nomenclature proposal for SARS-CoV-2 lineages to assist genomic epidemiology. Nat. Microbiol. *5*, 1403–1407.

Rana, K., Mohindra, R., and Pinnaka, L. (2021). Vaccine breakthrough infections with SARS-CoV-2 variants. N. Engl. J. Med. *385*, e7.

Reitter, J.N., Means, R.E., and Desrosiers, R.C. (1998). A role for carbohydrates in immune evasion in AIDS. Nat. Med. *4*, 679–684.

Saito, A., Irie, T., Suzuki, R., Maemura, T., Nasser, H., Uriu, K., Kosugi, Y., Shirakawa, K., Sadamasu, K., Kimura, I., et al. (2021). Enhanced fusogenicity and pathogenicity of SARS-CoV-2 Delta P681R mutation. Nature. https://doi.org/10.1038/s41586-021-04266-9.

Sato, K., Misawa, N., Fukuhara, M., Iwami, S., An, D.S., Ito, M., and Koyanagi, Y. (2012). Vpu augments the initial burst phase of HIV-1 propagation and downregulates BST2 and CD4 in humanized mice. J. Virol. *86*, 5000–5013.

Sato, K., Misawa, N., Iwami, S., Satou, Y., Matsuoka, M., Ishizaka, Y., Ito, M., Aihara, K., An, D.S., and Koyanagi, Y. (2013). HIV-1 Vpr accelerates viral replication during acute infection by exploitation of proliferating $CD4^+$ T cells *in vivo*. PLOS Pathog. *9*, e1003812.

Sato, K., Misawa, N., Nie, C., Satou, Y., Iwakiri, D., Matsuoka, M., Takahashi, R., Kuzushima, K., Ito, M., Takada, K., et al. (2011). A novel animal model of Epstein-Barr virus-associated hemophagocytic lymphohistiocytosis in humanized mice. Blood *117*, 5663–5673.

Skehel, J.J., Stevens, D.J., Daniels, R.S., Douglas, A.R., Knossow, M., Wilson, I.A., and Wiley, D.C. (1984). A carbohydrate side chain on hemagglutinins of Hong Kong influenza viruses inhibits recognition by a monoclonal antibody. Proc. Natl. Acad. Sci. U S A. *81*, 1779–1783.

Suchard, M.A., Lemey, P., Baele, G., Ayres, D.L., Drummond, A.J., and Rambaut, A. (2018). Bayesian phylogenetic and phylodynamic data integration using BEAST 1.10. Virus Evol. *4*, vey016.

Touret, F., Luciani, L., Baronti, C., Cochin, M., Driouich, J.S., Gilles, M., Thirion, L., Nougairede, A., and de Lamballerie, X. (2021). Replicative fitness of a SARS-CoV-2 20I/501Y.V1 variant from lineage B.1.1.7 in human reconstituted bronchial epithelium. mBio *12*, e0085021.

Wagh, K., Hahn, B.H., and Korber, B. (2020). Hitting the sweet spot: exploiting HIV-1 glycan shield for induction of broadly neutralizing antibodies. Curr. Opin. HIV AIDS *15*, 267–274.

Wall, E.C., Wu, M., Harvey, R., Kelly, G., Warchal, S., Sawyer, C., Daniels, R., Adams, L., Hobson, P., Hatipoglu, E., et al. (2021). AZD1222-induced neutralising antibody activity against SARS-CoV-2 Delta VOC. Lancet. *398*, 207–209.

Wang, C.C., Chen, J.R., Tseng, Y.C., Hsu, C.H., Hung, Y.F., Chen, S.W., Chen, C.M., Khoo, K.H., Cheng, T.J., Cheng, Y.S., et al. (2009). Glycans on influenza hemagglutinin affect receptor binding and immune response. Proc. Natl. Acad. Sci. U S A. *106*, 18137–18142.

Wang, P., Casner, R.G., Nair, M.S., Wang, M., Yu, J., Cerutti, G., Liu, L., Kwong, P.D., Huang, Y., Shapiro, L., et al. (2021a). Increased resistance of SARS-CoV-2 variant P.1 to antibody neutralization. Cell Host Microbe. *29*, 747–751 e744.

Wang, P., Nair, M.S., Liu, L., Iketani, S., Luo, Y., Guo, Y., Wang, M., Yu, J., Zhang, B., Kwong, P.D., et al. (2021b). Antibody resistance of SARS-CoV-2 variants B.1.351 and B.1.1.7. Nature *593*, 130–135.

WHO. (2021a). Tracking SARS-CoV-2 variants.https://www.who.int/en/activities/tracking-SARS-CoV-2-variants/.

WHO. (2021b). WHO coronavirus (COVID-19) dashboard in Chile.https://covid19.who.int/region/amro/country/cl.

Wolfl, M., Kuball, J., Ho, W.Y., Nguyen, H., Manley, T.J., Bleakley, M., and Greenberg, P.D. (2007). Activation-induced expression of CD137 permits detection, isolation, and expansion of the full repertoire of $CD8^+$ T cells responding to antigen without requiring knowledge of epitope specificities. Blood *110*, 201–210.

Wrobel, A.G., Benton, D.J., Xu, P., Roustan, C., Martin, S.R., Rosenthal, P.B., Skehel, J.J., and Gamblin, S.J. (2020). SARS-CoV-2 and bat RaTG13 spike glycoprotein structures inform on virus evolution and furin-cleavage effects. Nat. Struct. Mol. Biol. *27*, 763–767.

Yan, R., Zhang, Y., Li, Y., Xia, L., Guo, Y., and Zhou, Q. (2020). Structural basis for the recognition of SARS-CoV-2 by full-length human ACE2. Science *367*, 1444–1448.

Yurkovetskiy, L., Wang, X., Pascal, K.E., Tomkins-Tinch, C., Nyalile, T.P., Wang, Y., Baum, A., Diehl, W.E., Dauphin, A., Carbone, C., et al. (2020). Structural and functional analysis of the D614G SARS-CoV-2 spike protein variant. Cell *183*, 739–751 e8.

Zahradník, J., Dey, D., Marciano, S., Kolářová, L., Charendoff, C.I., Subtil, A., and Schreiber, G. (2021a). A protein-engineered, enhanced yeast display platform for rapid evolution of challenging targets. Acs. Synth. Biol. *10*, 3445–3460.

Zahradnik, J., Marciano, S., Shemesh, M., Zoler, E., Harari, D., Chiaravalli, J., Meyer, B., Rudich, Y., Li, C., Marton, I., et al. (2021b). SARS-CoV-2 variant prediction and antiviral drug design are enabled by RBD in vitro evolution. Nat. Microbiol. *6*, 1188–1198.

## STAR★METHODS

### KEY RESOURCES TABLE

| REAGENT or RESOURCE | SOURCE | IDENTIFIER |
|---|---|---|
| **Antibodies** | | |
| Human anti-SARS-CoV-2 S monoclonal antibody (clone 4A8) | (Chi et al., 2020) | N/A |
| Human anti-SARS-CoV-2 S monoclonal antibody (clone COV2-2490) | (Liu et al., 2021c) | N/A |
| FITC-conjugated anti-human CD3 antibody | Biolegend | Cat# 300440; RRID: AB_2562046 |
| BV510-conjugated anti-human CD3 antibody | Biolegend | Cat# 317331; RRID: AB_2561376 |
| APC-Cy7-conjugated anti-human CD8 antibody | Biolegend | Cat# 301016; RRID: AB_314134 |
| PerCP-Cy5.5-conjugated anti-human CD14 antibody | Biolegend | Cat# 325622; RRID: AB_893250 |
| PerCP-Cy5.5-conjugated anti-human CD19 antibody | Biolegend | Cat# 302230; RRID: AB_2073119 |
| PE-Cy7-conjugated anti-human CD25 antibody | Biolegend | Cat# 356107; RRID: AB_2561974 |
| APC-conjugated anti-human CD137 antibody | Biolegend | Cat# 309809; RRID: AB_830671 |
| PE-conjugated anti-human IFN-γ antibody | BD Biosciences | Cat# 554552; RRID: AB_395474 |
| Anti-SARS-CoV-2 S S1/S2 rabbit polyclonal antibody | Thermo Fisher Scientific | Cat# PA5-112048; AB_2866784 |
| APC-conjugated anti-human IgG antibody | Biolegend | Cat #410712; RRID: AB_2565790 |
| Alexa Fluor 647-conjugated anti-rabbit IgG antibody | Thermo Fisher Scientific | Cat# A21244; RRID: AB_2535812 |
| **Biological samples** | | |
| Human sera (BNT162b2-vaccinated) | This study | N/A |
| Human PBMCs | This study | N/A |
| **Chemicals, peptides, and recombinant proteins** | | |
| Dulbecco's modified Eagle's medium (high glucose) | Wako | Cat# 044-29765 |
| RPMI1640 medium | Thermo Fisher Scientific | Cat# 11875101 |
| Expi293 expression medium | Thermo Fisher Scientific | Cat# A1435101 |
| Fetal calf serum (FCS) | Sigma-Aldrich | Cat# 172012-500ML |
| Penicillin streptomycin (PS) | Sigma-Aldrich | Cat# P4333-100ML |
| Ficoll-Paque Plus | GE Healthcare Life Sciences | Cat# 17-1440-03 |
| PrimeSTAR GXL DNA polymerase | Takara | Cat# R050A |
| DNA ligation kit "Mighty Mix" | Takara | Cat# 6023 |
| Acc65I | New England Biolab | Cat# R0599S |
| KpnI | New England Biolab | Cat# R0142S |
| NotI | New England Biolab | Cat# R1089S |
| BamHI | New England Biolab | Cat# R0136S |
| Lipofectamine 3000 | Thermo Fisher Scientific | Cat# L3000015 |
| PEI Max | Polysciences | Cat# 24765-1 |
| Bilirubin | Sigma-Aldrich | Cat# 14370-1G |
| CF640R succinimidyl ester | Biotium | Cat# 92108 |
| Recombinant human IL-2 | Peprotec | Cat# 200-02 |

(*Continued on next page*)

*Continued*

| REAGENT or RESOURCE | SOURCE | IDENTIFIER |
|---|---|---|
| NF9 peptide (NYNYLYRLF, residues 448-456 of the SARS-CoV-2 S protein) | (Motozono et al., 2021) | N/A |
| L452R peptide (NYNYRYRLF, L5R in NF9) | (Motozono et al., 2021) | N/A |
| L452Q peptide (NYNYQFRLF, L5Q in NF9) | This study | N/A |
| 7-aminoactinomycin D | Biolegend | Cat# 420404 |
| Paraformaldehyde | Nacalai Tesque | Cat# 09154-85 |
| Brefeldin A | Sigma-Aldrich | Cat# B7651 |
| Monensin | Biolegend | Cat# 420701 |
| Formaldehyde | Nacalai Tesque | Cat# 37152-51 |
| **Critical commercial assays** | | |
| One-Glo luciferase assay system | Promega | Cat# E6130 |
| ExpiFectamine 293 transfection kit | Thermo Fisher Scientific | Cat# A14525 |
| KAPA HiFi HotStart ReadyMix kit | Roche | Cat# KK2601 |
| Cytofix/Cytoperm Fixation/ Permeabilization solution kit | BD Biosciences | Cat# 554714 |
| **Experimental models: Cell lines** | | |
| Human: HEK293T cells | ATCC | CRL-3216 |
| Human: HOS cells | ATCC | CRL-1543 |
| Human: HOS-ACE2/TMPRSS2 cells | (Ferreira et al., 2021) | N/A |
| Human: HOS-ACE2 cells | (Saito et al., 2021) | N/A |
| Human: C1R-A2402 cells | (Karaki et al., 1993) | N/A |
| Human: Expi293 cells | Thermo Fisher Scientific | Cat# A1435101 |
| Yeast (*Saccharomyces cerevisiae*): strain EBY100 | ATCC | MYA-4941 |
| **Oligonucleotides** | | |
| Primers for the construction of pCAGGS-based S expression plasmids, see Table S6 | This study | N/A |
| Forward primer for the preparation of RBD L452Q expression plasmid (RBD_L452Q_F): GGA CAG CAA GGT GGG AGG CAA CTA CAA CTA CCA ATA CAG ACT GTT CAG GAA GAG CAA C | This study | N/A |
| Reverse primer for the preparation of RBD L452Q expression plasmid (pCT_seq reverse): CAT GGG AAA ACA TGT TGT TTA CGG AG | This study | N/A |
| Forward primer for the preparation of RBD F490S expression plasmid (RBD_int_F): CTA CAA ACT GCC TGA TGA CTT CAC | This study | N/A |
| Reverse primer for the preparation of RBD F490S expression plasmid (RBD_F490S_R): GGT TGG TTG GAA GCC ATA GGA TTG GAG TGG AGA GTA ACA GTT GAA GCC CTC CAC TCC | This study | N/A |
| Primer for the sequencing of the RBD expression plasmid (pCTCON_seq_F): GCA GCC CCA TAA ACA CAC AGT AT | This study | N/A |
| **Recombinant DNA** | | |
| Plasmid: pC-SARS2-S D614G | (Ozono et al., 2021) | N/A |
| Plasmid: pCAGGS | (Niwa et al., 1991) | N/A |
| Plasmid: pC-SARS2-S Alpha | This study | N/A |

(*Continued on next page*)

*Continued*

| REAGENT or RESOURCE | SOURCE | IDENTIFIER |
|---|---|---|
| Plasmid: pC-SARS2-S Beta | This study | N/A |
| Plasmid: pC-SARS2-S Gamma | This study | N/A |
| Plasmid: pC-SARS2-S Delta | This study | N/A |
| Plasmid: pC-SARS2-S Epsilon | (Motozono et al., 2021) | N/A |
| Plasmid: pC-SARS2-S Lambda | This study | N/A |
| Plasmid: pC-SARS2-S Lambda+N246-253RSYLTPGD | This study | N/A |
| Plasmid: pC-SARS2-S G75V | This study | N/A |
| Plasmid: pC-SARS2-S T76I | This study | N/A |
| Plasmid: pC-SARS2-S GT75-75VI | This study | N/A |
| Plasmid: pC-SARS2-S RSYLTPGD246-253N | This study | N/A |
| Plasmid: pC-SARS2-S L452Q | This study | N/A |
| Plasmid: pC-SARS2-S F490S | This study | N/A |
| Plasmid: pC-SARS2-S L452Q/F490S | This study | N/A |
| Plasmid: pC-SARS2-S Lambda N246A | This study | N/A |
| Plasmid: pC-SARS2-S Lambda N246Q | This study | N/A |
| Plasmid: pC-SARS2-S RSYLTPGD246-253A | This study | N/A |
| Plasmid: pC-SARS2-S RSYLTPGD246-253Q | This study | N/A |
| Plasmid: psPAX2-IN/HiBiT | (Ozono et al., 2020) | N/A |
| Plasmid: pWPI-Luc2 | (Ozono et al., 2020) | N/A |
| Plasmid: pLVSIN-CMV Hyg | Takara | Cat# 6182 |
| Plasmid: pLVSIN-CMV Hyg-Crimson | This study | N/A |
| Plasmid: pLVSIN-CMV Hyg-ZsGreen1 | This study | N/A |
| Plasmid: pHL-sec | Addgene | Cat# 99845 |
| Plasmid: pHL-sec-human ACE2 (residues 18-740) | (Zahradnik et al., 2021a) | N/A |
| Plasmid: pJYDC1 | Addgene | Cat# 162458 |
| Plasmid: pJYDC1-SARS-CoV-2 S RBD (residues 336-528) | (Zahradnik et al., 2021a) | N/A |
| Plasmid: pJYDC1-SARS-CoV-2 S RBD L452R | (Motozono et al., 2021) | N/A |
| Plasmid: pJYDC1-SARS-CoV-2 S RBD F490S | This study | N/A |
| Plasmid: pJYDC1-SARS-CoV-2 S RBD L452R/F490S | This study | N/A |
| Software and algorithms | | |
| MAFFT suite v7.467 | (Katoh and Standley, 2013) | https://mafft.cbrc.jp/alignment/software/ |
| IQ-TREE 2 v2.1.3 | (Minh et al., 2020) | N/A |
| BEAST v1.10.4 | (Suchard et al., 2018) | N/A |
| FigTree v1.4.4 | Andrew Rambaut | http://tree.bio.ed.ac.uk/software/figtree |
| Discovery Studio 2021 | Dassault Systèmes BIOVIA | N/A |
| MODELLER v9.24 | (Fiser et al., 2000) | N/A |
| Sequencher v5.1 | Gene Codes Corporation | N/A |
| Python v3.7 | Python Software Foundation | https://www.python.org |
| FlowJo | Tree Star | N/A |
| Prism 9 | GraphPad Software | https://www.graphpad.com/scientific-software/prism/ |

(*Continued on next page*)

*Continued*

| REAGENT or RESOURCE | SOURCE | IDENTIFIER |
|---|---|---|
| Other | | |
| GISAID | Freunde von GISAID e.V. | https://www.gisaid.org |
| Pangolin | (Rambaut et al., 2020) | https://cov-lineages.org/pangolin.html |
| 0.45-μm pore size filter | Thermo Fisher Scientific | Cat# 09-740-114 |
| HisTrap Fast Flow column | Cytiva | Cat# 17-5255-01 |
| Ultracel-3 regenerated cellulose membrane | Merck | Cat# UFC900324 |
| 20-μm pluriStrainer | PluriSelect | Cat# 43-50020-03 |

## RESOURCE AVAILABILITY

### Lead contact

Further information and requests for resources and reagents should be directed to and will be fulfilled by the Lead Contact, Kei Sato (KeiSato@g.ecc.u-tokyo.ac.jp).

### Materials availability

All unique reagents generated in this study are listed in the key resources table and available from the lead contact with a completed Materials Transfer Agreement.

### Data and code availability

- The data reported in this paper will be shared by the lead contact upon request.
- This paper does not report original code.
- Any additional information required to reanalyze the data reported in this paper is available from the lead contact upon request.

## EXPERIMENTAL MODEL AND SUBJECT DETAILS

### Ethics statement

For the use of human specimens, all protocols involving human subjects recruited at Kyoto University were reviewed and approved by the Institutional Review Boards of Kyoto University (approval number G0697) and Kumamoto University (approval numbers 2074 and 477) and The Institute of Medical Science, The University of Tokyo (approval number 2021-1-0416). All human subjects provided written informed consent.

### Collection of sera from BNT162b2-Vaccinated individuals

Peripheral blood was collected four weeks after the second vaccination with BNT162b2 (Pfizer-BioNTech), and the sera of 18 vaccinees (average age: 39.0 years, range: 28–59 years, 22% male. Average time between doses, 21.3 days. Average time of sampling after second vaccination, 26.3 days) were isolated from peripheral blood (Table S4). Sera were inactivated at 56°C for 30 min and stored at −80°C until use.

### Collection of human PBMCs

Human PBMCs were obtained from twelve HLA-A*24:02-positive BNT162b2-vaccinated donors (average age: 43 years, range: 32–67 years, 58% male), six HLA-A*24:02-negative BNT162b2-vaccinated donors (average age: 43 years, range: 32–58 years, 50% male), and six HLA-A24-positive unvaccinated seronegative donors (average age: 38 years, range: 32–44 years, 50% male) (Table S5). PBMCs were purified by density gradient centrifugation using Ficoll-Paque Plus (GE Healthcare Life Sciences, Cat# 17-1440-03) and stored in liquid nitrogen until further use.

### Cell culture

HEK293T cells (a human embryonic kidney cell line; ATCC CRL-3216) and HOS cells (a human osteosarcoma cell line; ATCC CRL-1543) were maintained in Dulbecco's modified Eagle's medium (high glucose) (Wako, Cat# 044-29765) containing 10% fetal calf serum (FCS) and 1% antibiotics (penicillin and streptomycin; PS). HOS-ACE2/TMPRSS2 cells, HOS cells stably expressing human ACE2 and TMPRSS2, were prepared as described previously (Ferreira et al., 2021; Ozono et al., 2021). HOS-ACE2 cells, HOS cells stably expressing human ACE2, were prepared as described previously (Saito et al., 2021). C1R cells expressing HLA-A*24:02 (C1R-A2402) (Karaki et al., 1993), kindly provided by Dr. Masafumi Takiguchi (Kumamoto University, Japan), were maintained in RPMI 1640

medium (Thermo Fisher Scientific, Cat# 11875101) containing 10% FCS and 1% PS. Expi293 cells (Thermo Fisher Scientific, Cat# A14527) were maintained in Expi293 expression medium (Thermo Fisher Scientific, Cat# A1435101).

## METHOD DETAILS

### Viral genome sequence analysis

All SARS-CoV-2 genome sequences and annotation information used in this study were downloaded from GISAID (https://www.gisaid.org) as of June 29, 2021 (2,084,604 sequences). We obtained the 1,908 genomes of SARS-CoV-2 Lambda variant (C.37 lineage based on the PANGO annotation) in the GISAID metadata. We confirmed that all of them are isolated from humans. To estimate when a Lambda variant harboring the RSYLTPGD246-253N deletion mutation in the S protein occurred, we screened 1,908 Lambda variants by removing genomes 1) containing more than 5 undetermined nucleotides at coding regions and 2) having an unknown sampling date. We then collected 644 and 49 viral genomes with and without the RSYLTPGD246-253N deletion mutation in the Lambda S protein. We used the Wuhan-Hu-1 strain isolated in China on December 31, 2019 (GenBank ID: NC_045512.2 and GISAID ID: EPI_ISL_402125) as the outgroup for tree inference. We aligned entire genome sequences by using the FFT-NS-1 program in MAFFT suite v7.407 (Katoh and Standley, 2013) and deleted gapped regions in the 5' and 3' regions. We constructed a phylogenetic tree using IQ-TREE 2 v2.1.3 software (Minh et al., 2020) with 1,000 bootstraps (Figure S1A). The GTR+G substitution model is utilized based on the BIC criterion. We found that several sequences without the RSYLTPGD246-253N mutation also clustered with the genomes carrying the RSYLTPGD246-253N mutation (Figure S1A), which could be due to reversible mutation(s) and/or recombination (Jackson et al., 2021). Thus, these sequences were excluded from further analysis.

To estimate the emergence time of the Lambda variant (C.37 lineage), we collected all Lambda sequences carrying the RSYLTPGD246-253N mutation that were sampled in 2020 (2 sequences) and randomly sampled 100 sequences in 2021. We also added the following 4 SARS-CoV-2 genomes as the outgroup: strain Wuhan-Hu-1 (GISAID ID: EPI_ISL_1532199, isolated on December 26, 2019), EPI_ISL_1093172 (isolated on August 25, 2020), and EPI_ISL_1534645 (isolated on November 30, 2020). Note that the two viral genomes isolated in Peru on August 25, 2020 (EPI_ISL_1532199 and EPI_ISL_1093172) were categorized in the B.1.1.1 lineage, although they were previously categorized as the C.37 lineage. We carefully examined these two sequences and found that they could be used as a sister group of the C.37 lineage. EPI_ISL_1534645 does not contain any typical mutations in the S protein, but it is close to the genuine Lambda variant (Figure S1A). Therefore, we included these four sequences in the analysis. We conducted Bayesian tip-dating analysis using BEAST v1.10.4 (Suchard et al., 2018). We used the GTR+Gamma model for the nucleotide substitution model. For the assumption of rate variations, we applied an uncorrelated relaxed clock, assuming that the distribution of rates followed a gamma distribution. We carefully reviewed the effective sample size of each parameter and confirmed that all were > 200. The time to the most recent common ancestor of the genuine Lambda variants was estimated to be 2020.7585 (95% HPD, 2020.245–2020.8525). A timetree was generated using TreeAnnotator software in the BEAST package and visualized by using FigTree v1.4.4 (Figures 1C and S1B). Reconstruction of the population history, namely, the change in effective population size over time (Figure 1D), was conducted by a Bayesian skyline plot using the same software and parameter settings with the Lambda sequences as noted in the tip-dating analysis.

### Protein structure homology model

All protein structural analyses were performed using Discovery Studio 2021 (Dassault Systèmes BIOVIA). In Figures 2C and 2D, the crystal structure of SARS-CoV-2 S (PDB: 6ZGE) (Wrobel et al., 2020) was used as the template, and 40 homology models of the SARS-CoV-2 S of the Lambda variant were generated using Build Homology Model protocol MODELLER v9.24 (Fiser et al., 2000). Evaluation of the homology models was performed using PDF total scores and DOPE scores and the best model for Lambda S was selected. In Figure S2E, the cocrystal structure of SARS-CoV-2 and human ACE2 (PDB: 6M17) (Yan et al., 2020) was used.

### Plasmid construction

Plasmids expressing the SARS-CoV-2 S proteins of the parental (B.1) (Ozono et al., 2021) and the Epsilon (B.1.427) variant (Motozono et al., 2021) were prepared in our previous studies. Plasmids expressing the S proteins of the Alpha (B.1.1.7), Beta (B.1.351), Gamma (P.1), Delta (B.1.617.2), and Lambda (C.37) variants and the point mutants were generated by site-directed overlap extension PCR using pC-SARS2-S D614G (Ozono et al., 2021) as the template and the following primers listed in Table S6. The resulting PCR fragment was digested with Acc65I or KpnI and NotI and inserted into the corresponding site of the pCAGGS plasmid (Niwa et al., 1991). To construct the plasmids expressing fluorescent proteins (Crimson or ZsGreen1), pLVSIN-CMV Hyg plasmid (Takara, Cat# 6182) was digested with NotI and BamHI and the DNA fragment encoding Crimson or ZsGreen1 was inserted using a DNA ligation kit "Mighty Mix" (Takara, Cat# 6023). Nucleotide sequences were determined by DNA sequencing services (Fasmac or Eurofins), and the sequence data were analyzed by Sequencher v5.1 software (Gene Codes Corporation).

### Pseudovirus assay

Pseudovirus assays were performed as previously described (Motozono et al., 2021; Ozono et al., 2021). Briefly, for pseudoviruses, lentivirus (HIV-1)-based, luciferase-expressing reporter viruses pseudotyped with the SARS-CoV-2 S protein and its derivatives, HEK293T cells ($1 \times 10^6$ cells) were cotransfected with 1 μg psPAX2-IN/HiBiT (Ozono et al., 2020), 1 μg pWPI-Luc2 (Ozono et al.,

2020), and 500 ng plasmids expressing parental S or its derivatives using Lipofectamine 3000 (Thermo Fisher Scientific, Cat# L3000015) or PEI Max (Polysciences, Cat# 24765-1) according to the manufacturer's protocol. At two days posttransfection, the culture supernatants were harvested and centrifuged. The amount of pseudoviruses prepared was quantified using the HiBiT assay as previously described (Ozono et al., 2020, 2021). The pseudoviruses prepared were stored at −80°C until use. For the experiment, HOS-ACE2 cells and HOS-ACE2/TMPRSS2 cells (10,000 cells/50 μL) were seeded in 96-well plates and infected with 100 μL of pseudoviruses prepared at 4 different doses. At two days postinfection, the infected cells were lysed with a One-Glo luciferase assay system (Promega, Cat# E6130), and the luminescent signal was measured using a CentroXS3 plate reader (Berthhold Technologies) or GloMax explorer multimode microplate reader 3500 (Promega).

For competition assay (Figure S2C), pLVSIN-CMV Hyg vectors (Takara, Cat# 6182) encoding fluorescent proteins (Crimson or ZsGreen1) were used to prepare the pseudoviruses bearing Lambda S or Lambda+N246-253RSYLTPGD S. Briefly, HEK293T cells were cotransfected with psPAX2-IN/HiBiT (800 ng), the Lambda S expression plasmid (400 ng), and pLVSIN-CMV Hyg-Crimson (800 ng) or psPAX2-IN/HiBiT (800 ng), the Lambda+N246-253RSYLTPGD S expression plasmid (400 ng), and pLVSIN-CMV Hyg-ZsGreen1 (800 ng). For the experiment, HOS-ACE2/TMPRSS2 cells (10,000 cells/50 μl) were seeded in 96-well plates and infected with a Crimson-expressing reporter virus pseudotyped with Lambda S and a ZsGreen1-expressing reporter virus pseudotyped with Lambda+N246-253RSYLTPGD S (at 2,000 ng p24 antigen each). At two days postinfection, the infected cells were fixed with 1% paraformaldehyde (Nacalai Tesque, Cat# 09154-85), and the levels of fluorescent protein expression were analyzed by flow cytometry using a FACSCalibur (BD Biosciences). The data obtained by flow cytometry were analyzed with FlowJo software (Tree Star).

### Antibody treatment

Antibody treatment for neutralization and infectivity enhancement was performed as previously described (Saito et al., 2021). Briefly, this assay was performed on HOS-ACE2/TMPRSS2 cells using SARS-CoV-2 S pseudoviruses expressing luciferase (see "pseudovirus assay" above). SARS-CoV-2 S pseudoviruses (counting ~20,000 relative light units) were incubated with serially diluted heat-inactivated human sera, the NTD-targeting NAb clone 4A8 (Chi et al., 2020) or the EAb clone COV2-2490 (Liu et al., 2021c) at 37°C for 1 h. Pseudoviruses without sera/antibodies were included as controls. Then, an 80 μl mixture of pseudovirus and sera/antibodies was added to HOS-ACE2/TMPRSS2 cells (10,000 cells/50 μl) in a 96-well white plate, and the luminescence was measured as described above (see "pseudovirus assay" above). A 50% neutralization titer was calculated using Prism 9 (GraphPad Software).

### Yeast surface display

Soluble human ACE2 was prepared as previously described (Motozono et al., 2021; Zahradnik et al., 2021a). Briefly, the expression plasmid for the extracellular domain of human ACE2 (residues 18-740) based on pHL-sec (Addgene, Cat# 99845) (Zahradnik et al., 2021a) was transfected into Expi293 cells using an ExpiFectamine 293 transfection kit (Thermo Fisher Scientific, Cat# A14525) according to the manufacturer's protocol. Expression enhancer was added 16 h posttransfection and the expression continued for an additional three days. Subsequently, the culture medium was harvested, centrifuged, filtered through a 0.45-μm pore size filter (Thermo Fisher Scientific, Cat# 09-740-114), and the protein was purified by a 5-ml HisTrap Fast Flow column (Cytiva, Cat# 17-5255-01) using a ÄKTA pure chromatography system (Cytiva). The purified protein was concentrated in PBS by using an Ultracel-3 regenerated cellulose membrane (Merck, Cat# UFC900324). The batch-to-batch reproducibility was assessed using a Tycho NT.6 system (NanoTemper).

A yeast-based SARS-CoV-2 RBD expression system was prepared as previously described (Motozono et al., 2021; Zahradnik et al., 2021b). Briefly, the plasmid pJYDC1 (Addgene, Cat# 162458) (Zahradnik et al., 2021b) encoding the SARS-CoV-2 S RBD (residues 336-528) (pJYDC1-RBD) (Zahradnik et al., 2021a) was modified by the restriction enzyme-free cloning procedure (Peleg and Unger, 2014). Megaprimers for targeted mutagenesis were amplified by PCR using the KAPA HiFi HotStart ReadyMix kit (Roche, Cat# KK2601) with the following pairs of primers according to the manufacturer's protocol: RBD_L452Q_F, 5'-GGA CAG CAA GGT GGG AGG CAA CTA CAA CTA CCA ATA CAG ACT GTT CAG GAA GAG CAA C-3'; pCT_seq reverse, 5'-CAT GGG AAA ACA TGT TGT TTA CGG AG-3'; RBD_int_F, 5'-CTA CAA ACT GCC TGA TGA CTT CAC-3'; and RBD_F490S_R, 5'-GGT TGG TTG GAA GCC ATA GGA TTG GAG TGG AGA GTA ACA GTT GAA GCC CTC CAC TCC-3'. In addition, pCTCON_seq_F: 5'-GCA GCC CCA TAA ACA CAC AGT AT-3' was used for sequencing. The PCR products were integrated into pJYDC1 by integration PCR as previously described (Motozono et al., 2021; Peleg and Unger, 2014). The double mutant L452Q/F490S was prepared using F490S megaprimers and pJYDC1-RBD L452Q as the template.

An enhanced yeast surface display to analyze the binding affinity of the SARS-CoV-2 S RBD variants for human ACE2 was performed as previously described (Motozono et al., 2021). Briefly, the pJYDC1-based yeast display plasmids were transformed into yeast (*Saccharomyces cerevisiae*; strain EBY100, ATCC MYA-4941) by the LiAc-PEG method and selected by growth on SD-W plates (Peleg and Unger, 2014). Single colony cultures grown in 1 ml of liquid SD-CAA medium (Zahradnik et al., 2021a) overnight at 30°C (220 rpm), were used to inoculate expression 1/9 medium (Zahradnik et al., 2021a) with 1 nM bilirubin (Sigma-Aldrich, Cat# 14370-1G). The cells, washed with PBS-B buffer [PBS supplemented with bovine serum albumin (1 g/l)], were aliquoted into solutions (1-100 ml, (Zahradnik et al., 2021b) consisting of PBS-B buffer with 12 – 14 different concentrations (ranging from 20 nM to 25 pM) of the CF640R succinimidyl ester (Biotium, Cat# 92108) labeled human ACE2 protein (residues 18-740) and incubated overnight. Subsequently, the yeast cells were washed with PBS-B buffer and passed through a 20-μm pluriStrainer® (PluriSelect, Cat# 43-50020-03), after which the binding signal of CF640R-labeled human ACE2 protein (residues 18-740) attached to

yeasts was analyzed using an S3e Cell Sorter device (Bio-Rad, USA). The fluorescent signal was processed and fitted to the standard noncooperative Hill equation by nonlinear least-squares regression using Python v3.7 (https://www.python.org) as previously described (Zahradnik et al., 2021b).

### Activation-induced marker assay

Activation-induced marker assay was performed as previously described (Motozono et al., 2021). Briefly, expansion of antigen-specific human $CD8^+$ T cells and the analysis of the surface expression levels of the activation markers CD25 and CD137 were performed as previously described (Motozono et al., 2021; Wolfl et al., 2007). Briefly, human PBMCs were pulsed with 100 nM NF9 peptide (NYNYLYRLF, residues 448-456 of the SARS-CoV-2 S protein; synthesized by Scrum, Inc.) and maintained in RPMI 1640 medium (Thermo Fisher Scientific, Cat# 11875101) containing 10% FCS and 30 U/ml recombinant human IL-2 (Peprotec, Cat# 200-02) for 10-14 days. The *in vitro* expanded $CD8^+$ T cells (i.e., CTL lines) were restimulated with or without the NF9 peptide. After incubation at 37°C for 24 h, the cells were washed, and surface proteins (CD3, CD8, CD14, CD19, CD25 and CD137) were stained with the antibodies listed in key resources table. Dead cells were stained with 7-aminoactinomycin D (Biolegend, Cat# 420404). After incubation for 20 min on ice, the cells were fixed with 1% paraformaldehyde (Nacalai Tesque, Cat# 09154-85), and the levels of protein surface expression were analyzed by flow cytometry using a FACSCanto II (BD Biosciences). The data obtained by flow cytometry were analyzed with FlowJo software (Tree Star).

### Intracellular cytokine staining

Intracellular cytokine staining was performed as previously described (Motozono et al., 2021). Briefly, C1R-A2402 cells were pulsed with or without the NF9 peptide or its derivatives [the NF9-L452Q peptide (NYNYQYRLF, L5Q in NF9) and the NF9-L452Q peptide (NYNYRYRLF, L5R in NF9); synthesized by Scrum, Inc.] at concentrations from 0.1 to 10 nM at 37°C for 1 h. The cells were washed twice with PBS, mixed with the CTL lines generated from vaccinated or nonvaccinated donors (see above) and incubated with RPMI 1640 medium (Thermo Fisher Scientific, Cat# 11875101) containing 10% FCS and 5 μg/ml brefeldin A (Sigma-Aldrich, Cat# B7651) in a 96-well U plate at 37°C for 5 h. The cells were washed, and surface proteins (CD3, CD8, CD14 and CD19) were stained with the antibodies listed in key resources table. Dead cells were stained with 7-aminoactinomycin D (Biolegend, Cat# 420404). After incubation at 37°C for 30 min, the cells were fixed and permeabilized with a Cytofix/Cytoperm Fixation/Permeabilization solution kit (BD Biosciences, Cat# 554714); IFN-γ was stained with the antibodies listed in key resources table. After incubation at room temperature for 30 min, the cells were washed, and the levels of protein expression were analyzed by flow cytometry using a FACSCanto II (BD Biosciences) followed by analysis using FlowJo software (Tree Star).

### Flow cytometry

Flow cytometry was performed as previously described (Sato et al., 2011, 2012, 2013). Briefly, the HEK293T cells transfected with the plasmids for the expression of S derivatives were washed with PBS and incubated with 4A8 antibody (Chi et al., 2020), COV2-2490 antibody (Liu et al., 2021c), or an anti-SARS-CoV-2 S S1/S2 polyclonal antibody (Thermo Fisher Scientific; Cat# PA5-112048) at 4°C for 30 min. The cells were washed with PBS twice and stained with an APC-conjugated anti-human IgG monoclonal antibody (Biolegend; Cat #410712) or an Alexa Fluor 647-conjugated anti-rabbit IgG antibody (Thermo Fisher Scientific; Cat# A21244) at 4°C for 30 min. The cells stained with the fluorescent-labeled antibodies were washed with PBS twice and fixed with 4% formaldehyde (Nacalai Tesque, Cat# 37152-51) in PBS. Flow cytometry was performed using a FACSCalibur (BD Biosciences) followed by analysis using FlowJo software (Tree Star).

## QUANTIFICATION AND STATISTICAL ANALYSIS

Data analyses were performed using Prism 9 (GraphPad Software). Data are presented as average with SD.